# UV AND IR MATRIX ASSISTED LASER DESORPTION/IONIZATION USING AXIAL AND ORTHOGONAL INJECTION TIME-OF-FLIGHT MASS SPECTROMETERS

By

Maciej Piotr Jan Bromirski

A Thesis
Submitted to the Faculty of Graduate Studies
in partial Fulfillment of the Requirements
for the Degree of

Master of Science

Department of Physics and Astronomy
University of Manitoba
Winnipeg, Manitoba, Canada

August 2002

THE UNIVERSITY OF MANITOBA

FACULTY OF GRADUATE STUDIES

*****

COPYRIGHT PERMISSION PAGE

# UV AND IR MATRIX ASSISTED LASER DESORPTION/IONIZATION USING AXIAL AND ORTHOGONAL INJECTION TIME-OF-FLIGHT MASS SPECTROMETERS

BY

MACIEJ PIOTR JAN BROMIRSKI

A Thesis/Practicum submitted to the Faculty of Graduate Studies of The University of Manitoba in partial fulfillment of the requirements of the degree of

Master of Science

# ACKNOWLEDGEMENTS

I would like to thank my supervisor, Dr. Werner Ens, for his continuous help, patience, and advice in my research projects. I am grateful to Dr. K.G. Standing for accepting me into his lab and supporting my research.

I would like to thank Dr. R.C. Beavis also on my advisory committee, for his helpful suggestions and comments.

I am grateful to my colleagues Eric van Uytven, Ragnar Dworschak, Marek Znamirowski, Colin Lee and Julian Saba who made my studies more entertaining and enjoyable.

I would like to thank Dr. Alexander Loboda, Victor Spicer and Gilles Roy for their support, brilliant ideas and inspirations. Alexander and Victor were always eager to help whenever a computer crashed, or if something broke or blew up.

Most of the work presented in Chapter 2 was performed at Sciex during the summer of 2001 in partial fulfillment of an NSERC industrial scholarship. I worked at Sciex for 10 weeks under the supervision of Dr. Alexander Loboda. I would like to thank Sciex for giving me the opportunity to conduct my studies there and would especially like to thank Dr. Loboda for many dynamic conversations and productive experiments.

In Chapter 3, I present the work done in a joint collaboration between the Manitoba group, Dr. Stefan Berkenkamp and Dr. Franz Hillenkamp. This collaboration lead to several conference presentations and will be published in the near future. I would especially like to thank Stefan for sharing his experience and knowledge in DNA analysis.

Most importantly I would like to acknowledge my parents and my brother whom I love very much for their love, patience and devotion. In good times and bad times they have always supported me to the end. I would like to dedicate this thesis to them.

# ABSTRACT

This thesis is divided into four different chapters, ranging from fundamental studies of matrix-assisted laser desorption/ionization (MALDI) to practical applications of time-of-flight mass spectrometry (TOF-MS) for the study of bio-molecules.

The limiting factor for better performance of the ultraviolet-MALDI orthogonal injection mass spectrometers in the high *m/z* range is mainly due to metastable fragmentation of analyte in the q0 region. We show that the degree of metastable fragmentation can be controlled by changing the pressure of the cooling gas in the immediate vicinity of the target. A much higher pressure, created by a differential pressure gradient (cone), near the target effectively cools MALDI ions. As a result significant reduction of metastable fragmentation is observed. However, a higher-pressure results in increased formation of matrix adducts. Such matrix adducts were found to be effectively removed by increasing the de-clustering voltage between the target and the cone. In addition, matrix adducts formed by UV-MALDI ion source at elevated pressures can also be removed by increasing the temperature of the cooling gas up to +220 °C.

The amount of matrix adducts created in UV-MALDI process at elevated pressure was found to be a function of laser attenuation and the size of the laser spot on the target. The number of adducts and its intensity spread with increased laser energy. However, smaller laser spot size on the target created fewer number of adducts. The degree of adduct formation is independent of wavelength in the range of 337 to 355 nm.

Infrared-MALDI ion source at normal or elevated pressures produces much cooler ions than UV-MALDI. The cooler ions show no fragmentation, though matrix, sodium and potassium adducts produce extensive high mass tails and limit the quality of the spectrum. Sodium adducts are easily suppressed with the help of ion exchange beads, and matrix adducts are removed by increasing the temperature of the cooling gas.

Moreover, IR-MALDI using a glycerol matrix produces much higher charge states (up to +5) than are observed in UV-MALDI in a QqTOF instrument. This is an important advantage because it avoids the practical difficulties of introducing a high accelerating voltage or post-acceleration to obtain acceptable detection efficiency, and duty cycle.

A compact, low-power, high repetition rate (10 kHz) passively-Q-switched Nd:YAG laser (NanoUV-355) has been tested for use in MALDI in a conventional linear time-of-flight mass spectrometer (axial-TOF) and in an orthogonal-injection TOF instrument (QqTOF). It was found that the average number of ions produced per pulse was quite small and we speculate that most of the ions were produced in a small fraction of the laser pulses. As a result only a integrating transient recorder (ITR) gave reasonable data with the linear TOF. However, in the QqTOF instrument the performance of the NanoUV laser was comparable to the standard $N_2$ laser used for normal operations. This is because the injection pulse rate in the QqTOF instrument is similar to the laser repetition rate, so the average number of ions would be similar to the data obtained with axial TOF. In addition, the QqTOF introduces considerable attenuation and smoothes out the variation in the number of ions per pulse and allows a 4-channel TDC to be used.

Two other high repetition rate Nd:YAG lasers have been evaluated for the analysis of biomolecules in single and tandem MS. These lasers produce considerably higher energy per pulse at several kHz than the NanoUV and are suitable for MALDI.

Ultraviolet MALDI has proven to be powerful ion source for the study of intact bio-polymers, such as peptides, proteins and DNA. The MALDI ion source however, is only effective when coupled to a time-of-flight mass spectrometer. In tandem, a powerful tool is obtained for biological research but also for fundamental physics studies.

# TABLE OF CONTENTS

# CHAPTER 1

## Introduction

Mass spectrometry (MS) has become an important tool in biochemistry and biotechnology especially for the analysis of bio-polymers such as peptides, proteins, glycans and oligonucleotides. The application of MS is mainly possible because of the discovery of two ionization techniques; matrix-assisted laser desorption/ionization (MALDI) and electrospray ionization (ESI), both of which can produce intact molecular ions up to several hundred kilodalton.

MALDI and ESI produce ion beams that have different characteristics, and as a result different types of mass analyzers are typically employed to examine the ion beams. ESI produce a continuous beam of ions and thus is easily adapted to mass spectrometers that operate in continuous mode, such as quadrupole mass filters and ion traps. Unlike ESI, MALDI ions produced from a pulsed laser are suitably coupled to time-of-flight (TOF) mass analyzers, which require a well-defined start time.

A detailed description of both MALDI and ESI ion sources is presented in the following two sections, followed by an explanation of the principles of axial and orthogonal time-of-flight mass analyzer.

### 1.1 MALDI ion source

The basic concept involved in MALDI was independently and almost simultaneously discovered in the late 80's, by two groups: M. Karas and F. Hillenkamp [1] and by Tanaka [2]. This technique utilizes a pulsed laser to desorb and ionize molecules, particularly bio-molecules embedded in a suitable matrix. A schematic diagram of a typical MALDI ion source is illustrated in Fig. 1-1. First, a matrix used for

MALDI is chosen, since the type of matrix depends on the application. Tanaka used a fine metallic powder for their experiments, but the technique is now applied mainly with organic matrices such as nicotinic acid used first by Hillenkamp and Karas. The most common matrices are; sinapinic acid (SA) 3,5-dimethoxy-4-hydroxycinnamic acid, alpha-cyano-4-hydroxycinnamic acid (CHCA), gentisic acid (DHB) 2,5-dihydroxybenzoic acid, ferulic acid 4-hydroxy-3-methoxycinnamic acid, nicotinic acid-N-oxide, picolinic acid (PA) 2-pyridine carboxylic acid, 2,4-hydroxy-phenlyazo-benzoic acid (HABA) and 3-hydroxypicolinic acid (3HPA) 3-hydroxy-2-pyridinecarboxylic acid. These matrices are referred to as solid matrices. Glycerol is a typical liquid matrix used for infrared MALDI. Next, a sample of interest, such as peptides, proteins, DNA, RNA, antibodies, oligosaccharides etc., is mixed with a matrix and then a small quantity of it is deposited on the target and let dry. The dried sample on the target is then placed into vacuum. Finally, the sample is exposed to a pulse of light ranging from ultraviolet to infrared wavelengths and ions are created.

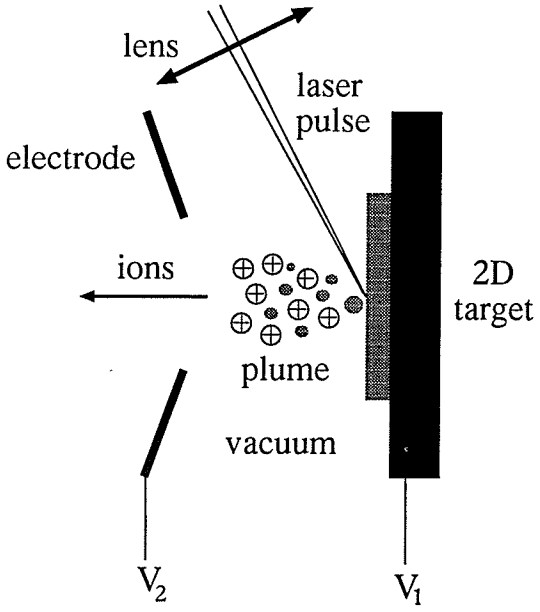


**Figure 1-1**. Schematic diagram of a MALDI ion source. Positive ions are extracted to the spectrometer if voltage $V_1$ is greater than $V_2$ this is known as positive mode. If the sign of $V_1$ and $V_2$ is reversed, negative ions are extracted to the spectrometer, this is known as negative mode of operation.

There is no accepted standard model describing the full mechanism of the matrix assisted laser desorption/ionization process. Nevertheless, there have been numerous theories that partially describe desorption and ionization processes [3,4,5,6], and a general consensus has emerged about the basic features. Matrix molecules absorb laser energy. The excess energy on the target results in an explosion and ejection of a matrix and analyte molecules and clusters. The rapidly expanding plume contains neutral and charged analyte molecules that are carried along with the matrix matter [7]. The ionization of the analyte is presumably due to ion-molecular reactions in the evolving plume [5]. The specific charge on the analyte molecules that are extracted into the analyzer depends on the mode of operation. In the positive mode of operation, where $V_1$ is more positive than $V_2$ see Fig. 1-1, positive ions are extracted. Typically, small molecular ions are singly charged by an addition of one proton and heavier molecules may contain up to a few extra charges. In the negative mode of operation, $V_1$ is less than $V_2$, negative ions are created by single or multiple proton detachment. Regardless of the mode of operation, the matrix matter evaporates or sublimes immediately ejecting mainly individual molecules and small clusters, leaving isolated analyte molecules, some of which may have an adduct or two. Subsequent collisions provide cooling, but if the pressure is high enough it will actually form adducts during expansion. The number of ions produced per laser pulse strongly depends on the laser fluence, matrix substrate and the sample preparation technique.

## 1.2 ESI ion source

In 1968 Malcolm Dole showed that intact ions of macromolecules could be introduced into the gas phase directly from solution using an electrospray source. The technique was used extensively for polymers like poly(ethylene) glycol in the early 1980s by Fenn *et al.* Dramatic progress for applications to large biolmolecules was made in the late 1980s by Fenn et al. [8], and by Aleksandrov *et al.* [9] Fenn used a quadrupole mass spectrometer,

whereas Alexandrov's early results were with a magnetic sector instrument. The ESI-MS ion source proved to be a powerful tool for bio-technology when non-covalent complexes up to 1 MDa in mass were analyzed.

ESI is a continuous ion source that produces highly charged molecular ions. Fig.1-2 shows a schematic diagram of a conventional atmospheric pressure ESI source.

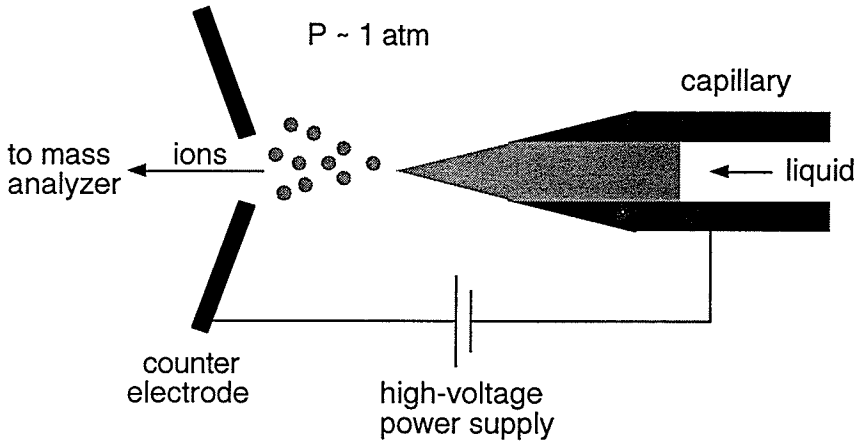


**Figure 1-2.** A schematic diagram of the typical layout of an electrospray ion source.

A solution containing an analyte is delivered through a thin conducting capillary ranging from ~100 μm (conventional ESI) to ~1-10 μm (nano-spray) ID sharpened at the end. The respective range of flow rate of the sprayed liquid is 1 mL/min to 20 nL/min. The capillary tip is normally placed about 1 cm from the counter electrode. The potential difference applied between the capillary tip and the counter electrode ranges from 2 to 5 kV resulting in strong electric field on the order of $10^4$ to $10^5$ V/cm. The polarity of the applied voltage determines the sign of the ions formed, i.e. positive or negative mode of ion source operation.

The strong electric fields cause formation of a Taylor's cone of the liquid at the tip, which emits small droplets of the solution. These droplets undergo evaporation while moving towards a counter electrode. A small orifice of the counter electrode is used to admit ions formed during evaporation process together with un-evaporated droplets and

surrounding gas. The ions enter the first vacuum chamber of an atmosphere/high vacuum interface and hence coupling the ion source with a mass analyzer.

In ESI, large charged droplets are produced by pneumatic nebulization; i.e. the forcing of the analyte solution through a needle, at the end of which is applied a potential. The potential used is sufficiently high to disperse the emerging solution into a very fine spray of charged droplets all at the same polarity. The solvent evaporates away, shrinking the droplet size and increasing the charge concentration at the droplet's surface. Eventually, at the Rayleigh limit, Coulombic repulsion overcomes the droplet's surface tension and the droplet explodes. This Coulombic explosion forms a series of smaller, lower charged droplets. The process of shrinking followed by explosion is repeated until individually charged analyte ions are formed. The charges are statistically distributed amongst the analyte's available charge sites, leading to the possible formation of multiply charged ions under the correct conditions.

## 1.3 Time-of-flight mass spectrometer: axial and orthogonal

TOF analyzers have many advantages for mass spectrometry of bio-molecules because of unlimited mass range, parallel detection, high sensitivity and high mass accuracy. Due to the pulsed nature of the MALDI, this source is naturally coupled to axial-TOF analyzers. However, for ESI, quadrupoles were initially more suitable because of the continuous nature; the high charge state brings the *m/z* value into the quadrupole range in most cases. Recently, orthogonal–injection TOF have enabled effective coupling of both ESI and MALDI sources. The axial and orthogonal TOF geometries are described below.

a) Axial MALDI

The simplest time-of-flight (TOF) mass spectrometer consists of an ion source on one end, a short source region 's' (where ions are accelerated in the presence of an electric field E), a linear drift region 'L' (free of electric field) and a detector at the other end.

This type of instrument requires a well-defined start time and position, hence the most useful ion source for such linear instrument is a pulsed source with a solid conducting sample target. Macfarlane and Torgerson were the first to exploit this with the introduction of plasma desorption mass spectrometry (PDMS) that uses fission fragments of MeV energy to radiate the sample [10]. Similarly, TOF is well suited as the analyzer for MALDI, which also uses a solid target and ionization by a pulsed laser. The MALDI target, with a sample to be analyzed is placed with its surface perpendicular to the axis of the TOF instrument. The MALDI ion plume is ejected along the axis of the instrument and the ions are extracted in the direction of the instrumental axis by a constant electric field. The ion flight time (t) is than measured over a linear flight path (L). The flight time is proportional to the square root of ion masses, as shown below:

$$t = \left(\frac{m}{2qV}\right)^{1/2} L \tag{1-1}$$

where qV is the kinetic energy acquired by ions during acceleration, see Fig. 1-3.

A mass spectrum is produced because ions of different mass will arrive at the detector at different times.

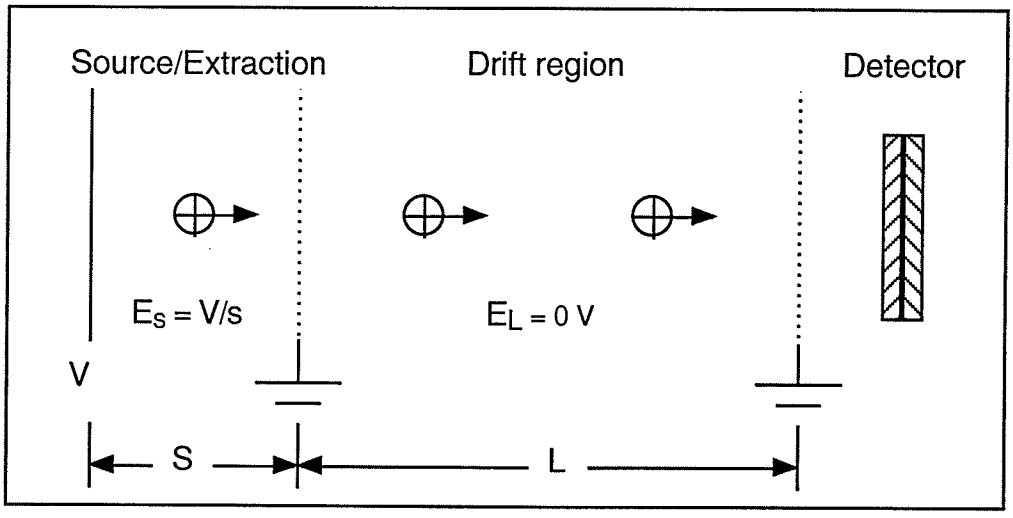


**Figure 1-3.** Schematic diagram of a linear time-of-flight mass spectrometer.

The advantage of such linear mass spectrometer is the essentially unlimited mass range and high sensitivity. MALDI linear TOF has been successful in mass measurements of proteins with molecular weights exceeding 1 MDa. Unfortunately, MALDI produces ions with a large energy (velocity) spread which gives rise to a considerable spread of times of flight, and thus to deterioration in mass resolution. A modification to the instrument that improved this problem was the introduction of an electrostatic ion mirror, proposed by Mamyrin in 1978 [11].

The simplest design of an electrostatic ion mirror is shown in Fig. 1-4. Ions extracted from the source travel freely (a distance $L_1$) from the object plane until they enter a uniform retarding electrostatic field $E = V/d$ (an ion mirror). The field in the ion mirror is created by a stacked rings connected to a voltage divider. Within the ion mirror the ions follow parabolic paths. Ions leave the mirror with velocity component parallel to the mirror axis ($v_z$) reversed. Finally, the ions once again travel freely to the detector (a distance $L_2$). The time spent in free flight is $L/v_z$ ($L = L_1 + L_2$), and the time spent in the mirror is $mv_z/2qE$. At the object plane ions have a distribution of velocities thus the velocity of any ion can be written as $v_z = v_0 + \delta$. The total time of flight expanded in Taylor series as a function of $(\delta/v_0)$ is:

$$t = \left(\frac{mv_0}{2qE} + \frac{L}{v_0}\right) + \left(\frac{\delta}{v_o}\right)\left(\frac{mv_0}{2qE} - \frac{L}{v_0}\right) + \ldots \qquad (1\text{-}2)$$

The first-order term in $\delta/v_0$ can be removed by setting $mv_o/2qE = L/v_o$, this implies that ion spends equal amounts of time in the drift and the ion mirror regions [12].

An ion mirror that eliminates the effect of a velocity variation $\delta$ to first order is know as single-stage ion mirror, that utilizes only one constant retarding field. Other ion mirrors including double-stage, quadratic and curved-field provide higher order focusing, however they are more complicated and are omitted in this discussion.

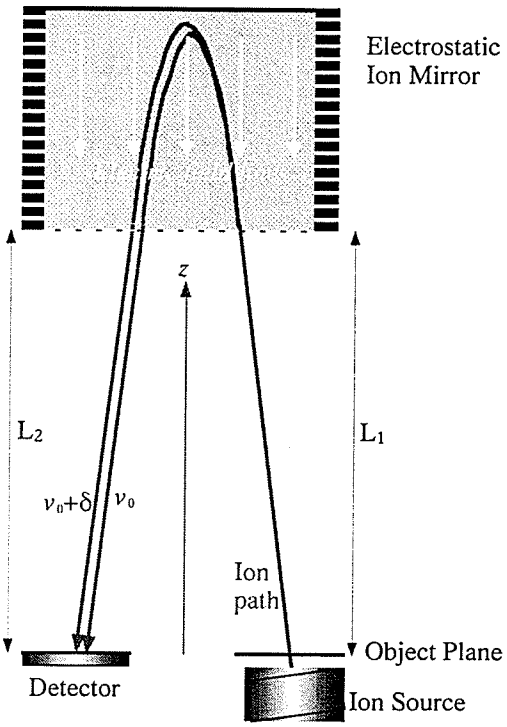


**Figure 1-4.** An illustration of the principle of a single-stage ion mirror to compensate for velocity spreads. Two ion paths are shown for axial velocities $v_z = v_0$ and $v_z = v_0 + \delta$. The ion with larger velocity spreads spends less time in the field-free region but more time in the mirror.

An electrostatic ion mirror corrects for time spreads that result from the velocity spread in the field-free region. However, it does not correct for time spreads produced by the velocity spread in the acceleration region and for this reason the mass resolution obtained in this geometry with direct extraction of MALDI ion was initially rather limited. To solve this problem a technique called time-lag focusing (TLF) is used. TLF or delayed extraction was developed during mid-fifties by Wiley and McLaren for extended gas sources [13]. This technique introduces a delay between the ion production and extraction, so that higher energy ions have traveled further into the acceleration region and therefore receive smaller extraction energy. The result is a packet near the source that has a small spatial spread, but large energy spread. But since this packet is now in field-free region and no further acceleration is required, the ion mirror can correct for the energy spread completely (in the ideal case) and image the packet on to the detector.

Delay extraction employed in the reflecting axial geometry reduces spatial and velocity distributions, and as a result mass resolutions ($M/\Delta M_{FWHM}$) greater than 20,000 can be obtained [14]. Despite the high mass resolution achievable with delay extraction, the technique has some limitations. First of all, good mass accuracy requires complicated calibration procedure. The focusing conditions depend on the type of matrix, the method of sample preparation, laser fluence and the intrinsic laser pulse width. More importantly, mass resolution can only be optimized for part of the spectrum at a time since the focusing condition depends on mass. Finally, delay extraction has had limited success in improving the mass resolution for masses above about 20 kDa. This is mainly due to fragmentation in the drift region (after the ions have left the source) that result from metastable decomposition or from unexpected collisions (processes known as post-source decay: PSD) with background gas.

b) Orthogonal-injection

The mass analysis of ions produced from a continuous source can greatly benefit from the features of TOF instruments. For example, ESI is the most successful technique for producing ions from intact non-covalent complexes that are formed with high *m/z* ratio. The *m/z* ratio of such complexes is beyond the range of quadrupole mass filters and thus require TOF that have unlimited mass range. Liquid chromatography is a separation technique that produces a continuous output and its applications are well suited with the high sensitivity and fast time response of TOF instruments. However, continues beam must be first formed into pulses before entering into the TOF spectrometer. This requirement is complicated and as a result the ions are injected into TOF with very low efficiency.

A much more efficient method of introducing the continuous beam of ions into TOF is achieved when the ions enter the TOF spectrometer perpendicular to its axis, a geometry known as 'orthogonal-injection', see Fig. 1-5. The ions pass through the ion

guide with low velocity and are injected into the flight path by the electrical pulses as indicated in Fig. 1-5. The interface consists of a set of RF quadrupoles operating typically at millitorr pressure. The combination of RF quadrupoles and buffer gas improves the ion beam quality by damping the initial velocity of the injected ions in the gas dynamic interface. Ions collide with the molecules of the buffer gas and lose their kinetic energy. The RF electric fields formed by quadrupoles create effective potential well that constrain radial motions of the ions. As ions lose their kinetic energy, they gradually "fall" to the bottom of the effective potential, slowly drifting along the axis of the quadrupoles. The collisional translational cooling produces a very thin beam of ions with very small velocity components in all directions. The cooled ions are accelerated and enter the TOF region through a small aperture.

Orthogonal-injection was first introduced in 1960s, but acquired particular importance when used with an electrospray source and an ion mirror first by Dodonov *et al.* [15] and then by Verentchikov *et. al.* [16]. This work was done to take the advantage of the decoupled ion source from TOF area, which provides a simple two-point calibration with optimum mass accuracy over the entire mass range. In addition, the decoupled source provides greater flexibility when experimenting with different source conditions.

For the same reason Krutchinsky *et al.* coupled MALDI ion source for the first time to an orthogonal-injection TOF mass spectrometer in 1998 [17]. In this geometry researchers are provided with greater flexibility when experimenting with different sample preparation methods and different laser wavelengths, pulse widths and fluence. In addition the orthogonal MALDI requires very little operation expertise because the optimum conditions are independent of mass and none of the adjustments required in axial MALDI are necessary.

Krutchinsky *et al.* found that best results with orthogonal MALDI were obtained with collisional cooling installed near the ion source. The collisional cooling interface is a

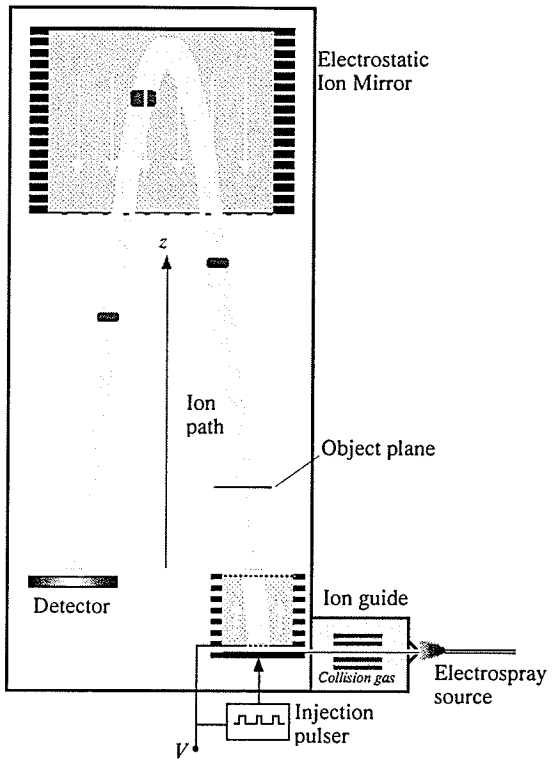


**Figure 1-5**. A schematic diagram of an orthogonal-injection TOF instrument with an ESI source. Collisional cooling is used in a quadrupole ion guide to produce a beam with a small energy spread, and a small cross section. The pressure in the ion guide is typically tens of millitorr; the main TOF chamber is typically $10^{-7}$ Torr. Ions are pulsed into the spectrometer at a repetition rate of several kilohertz; packets of ions for one mass are shown at several positions along the ion path.

set of RF operated quadrupoles immersed in an inert gas like $N_2$ that provides damping of the initial velocity of the MALDI ions and focuses them towards the center of the quadrupole axis. The collisions in the ion guide spread the ion pulse out along the quadrupole axis, producing a quasi-continuous beam, which can be treated like an electrospray beam.

The decoupled ion source from the TOF area allows for a quadrupole interface to be used not only as an ion guide but also as a mass filter to select a parent ion and with a gas cell the selected ion can be broken up to smaller pieces through a process known as collision-induced dissociation. The daughter ions produced from the breakup are then analyzed with TOF mass analyzer. Such combination of quadrupole and TOF leads to a

tandem mass spectrometer, which provides an efficient method of studying molecular structure such as amino acid sequence of peptides and proteins.

One such tandem instrument is the orthogonal-injection TOF-MS (QqTOF) equipped with a MALDI ion source constructed in our laboratory. The performance of this spectrometer is presented in the next section.

## 1.4 Performance of orthogonal MALDI QqTOF

- Single-MS mode (low mass range)

The performance of an orthogonal-injection time-of-flight mass spectrometer with collisional cooling (QqTOF a Sciex prototype of a QStar) and a MALDI ion source in single-MS mode is comparable to that of reflecting axial MALDI instruments with delayed extraction. However, in contrast to the sophisticated methods of calibration required in axial MALDI instruments, the accuracy in the QqTOF can be achieved over the entire spectrum with a simple 2-point calibration, and is not affected by ionization conditions, sample charging, or target irregularities.

In single-MS mode, the quadrupoles simply act as ion guides (RF only excitation), and the mass measurement is carried out in the TOF section of the instrument. The mass spectrum of a peptide mixture covering a range up to ~ 6000 Da is shown in Fig. 1-6. Resolving power (FWHM) of about 10,000 is observed for all four components. Here the raw data are shown without smoothing or pretreatment of any kind, as in all the other spectra presented in this thesis. Calibration is based on a simple quadratic equation and is usually calculated with two known mass peaks, although under some conditions only a single peak is needed. If an external calibration is carried out within about 30 minutes, a mass accuracy ~10 ppm is obtained in this mass range; accuracy in the range of a few ppm can be obtained using internal calibration.

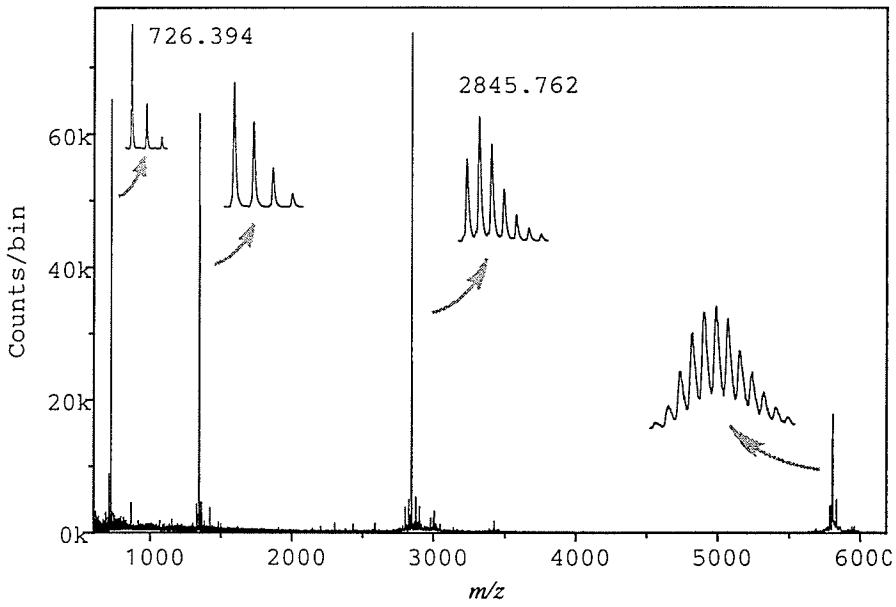


**Figure 1-6.** Positive ion spectrum of a mixture of dalargin, substance P, melittin, and insulin, showing a uniform resolving power M/ΔMFWHM of about 10,000 throughout the mass range. The mass calibration was performed using delargin and melittin with the masses indicated, and the mass determined for substance P (1347.738 Da) differs by only 2 ppm from its theoretical value.

In the mass range up to a few thousand daltons, the absolute uncertainty is within ~10 millidaltons. As a result of the decoupling of ion production from the measurement by collisional damping, the calibration is insensitive to the type of matrix used, the laser fluence, target irregularities, or sample charging.

To investigate the sensitivity limit of the instrument, 0.5 μL of 1.4 x $10^{-10}$M solution of Substance P (70 amol) was mixed with α-cyano 4-hydroxycinnamic acid (α-CHC) matrix and deposited onto the probe. In this case only, it was necessary to search the target to find a favorable portion that gave a useful signal-to-noise ratio. The resulting spectrum is shown in Fig. 1-7. The expanded segment of this spectrum shows that the sensitivity is limited by chemical noise that appears as resolved peaks at every mass, and not by a smooth background produced by electronic noise or unresolved metastable fragments, as is typical in axial MALDI TOF spectra.

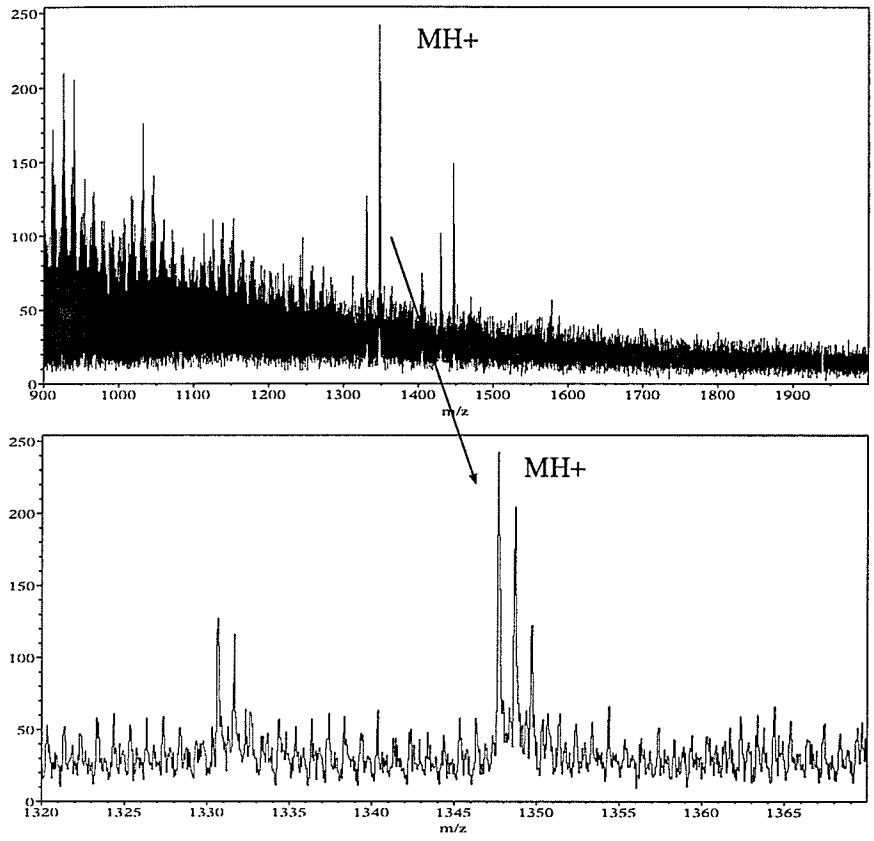


**Figure 1-7.** Positive ion spectrum of substance P obtained from a 70 amol sample deposited on the target, using DHB as the matrix. The spectrum is spotted in 1.25 ns bin, and was produced with 1200 laser shots, as described in the text.

- MS-MS mode

In the MS/MS mode, parent ions are selected in Q1 after cooling in q0, then broken up in q2 by collision-induced dissociation at low energy. The resulting daughter ions are measured in the TOF analyzer. The sensitivity of the QqTOF instrument in MS/MS mode for a test peptide like substance P is in the range of a few femtomoles (spectrum not shown). In MS/MS measurements, the quality of the daughter ion beam entering the TOF analyzer is similar to the quality of the parent ion beam observed in single-MS mode, so the daughter ions are measured with similar mass resolving power (~10,000) and mass accuracy (typically 10 ppm or better) for peaks of reasonable intensity.

# CHAPTER 2

## Orthogonal MALDI for high *m/z* range

### 2.1 Introduction

Sensitivity and mass accuracy of the MALDI-QqTOF mass spectrometer decreases rapidly for large proteins above 20 kDa. This is mainly due to metastable fragmentation in the MALDI ion plume and detection efficiency that decreases quickly for increasing *m/z*. The detection efficiency strongly depends on the magnitude of the acceleration voltage and for this reason the ions are usually accelerated to relatively high energies before they are incident on the detector. Axial MALDI TOF spectrometers typically use 30 kV acceleration voltage or more. However, orthogonal injection TOF instruments only operate at 4-10 kV acceleration voltage. In addition, sensitivity of orthogonal MALDI instrument is lower due to duty cycle losses and transmission losses of large molecular ions through the quadrupole section.

This present experiment investigates the metastable fragmentation and matrix-adduct formation of bio-molecules in UV-MALDI process by examining the dependence on fluence and spot size, as well as an extended examination of pressure and cone geometry, including pressures up to 2.5 Torr. Verentchikov originally reported preliminary experiments on metastable fragmentation in UV-MALDI at elevated ion source pressure in 1999 [1]. Factors causing fragmentation and adduct formation are presented in detail.

## 2.2 Experimental

Two different orthogonal-injection MALDI-TOF mass spectrometers were used to perform the following experiments. A QqTOF instrument was used for preliminary experiments, and the research was further investigated at MDS-Sciex using a prototype instrument Centaur.

a) QqTOF:

A schematic diagram of the MALDI-QqTOF spectrometer is shown in Fig. 2-1. The QqTOF instrument was originally developed with an electrospray ionization (ESI) source in collaboration with SCIEX [2, 3].

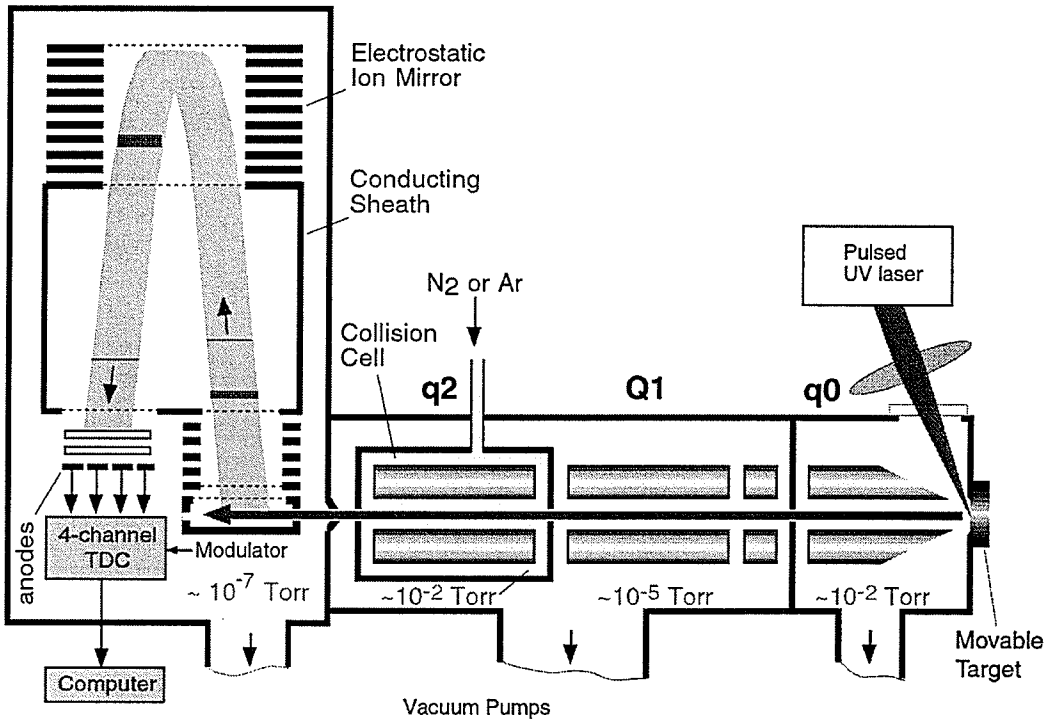


**Figure 2-1.** Schematic diagram of the MALDI QqTOF mass spectrometer. The UV laser is pulsed at a repetition rate between 1 Hz to 20 Hz. The resulting pulsed ion beam is converted to a quasi-continuous beam by collisional cooling in q0. The ion beam is injected into the mass spectrometer at a repetition rate of up to 10 kHz. The extent of the ion packet is illustrated by darker shading just after acceleration, at the object plane of the mirror, inside the mirror, and just prior to detection.

Samples are introduced on a MALDI target movable in 2 dimensional. Target movement is fully automated through a computer. The 2-D target is placed about 4 mm from the entrance of the quadrupole ion guide q0, and held at a potential of about 30 to 200 V above ground, depending on whether it is run in single-MS or MS/MS mode. The voltage on the target is approximately 10 V higher than q0, and for MS/MS analysis the voltage is ramped to 200V in order to produce more energetic and effective collisions with inert gas molecules. The pressure in this region is typically ~10 mTorr. Collisional cooling with $N_2$ gas in q0 converts the pulsed ion beam into a quasi-continuous beam with reduced radial and axial velocity distributions, suitable for introduction to the quadrupole mass filter, and subsequent orthogonal-injection into the TOF mass analyzer [4].

A $N_2$-laser (model VSL-337ND, Laser Science Inc.) has normally been used to irradiate the sample. It produces approximately 250 μJ of energy per pulse at 337 nm, and can be operated at repetition rates up to 20 Hz. The laser is coupled to a 200 μm diameter optical fiber (not shown) by a lens of 50 mm focal length. The output of the fiber is focused by two 100 mm focal length lenses to form an image of area ~ 0.3 $mm^2$ on the target.

MALDI produces mostly singly charged ions, so the detection efficiency can be considerably lower than for ESI, for heavy molecules. To reduce this problem, positive ions are accelerated from ground in the ion source to -10 kV at the final grid, giving an acceleration voltage of 10 kV. The conducting sheath enclosing the field-free drift region is also held at -10 kV. With this accelerating voltage, pulse repetition rates up to 10 kHz can be used for ions up to *m/z* ~ 3000. For higher *m/z*, the repetition rate must be reduced.

The repetition rate is adjusted to be equal to the reciprocal of the flight time of heaviest ion of interest.

A microchannel plate detector with 4-segment anodes is used to detect ions. Data are acquired using pulse-counting methods with a time-to-digital converter (TDCx4, IonWerks, Houston). The front of the detector is held at the same potential as the conducting shield, and the signal from each anode is taken out using custom-made isolation transformers. Measured flight times are transferred in list-mode from the TDC to a Power Macintosh computer using a FishCamp FPCI-DIO-96 digital I/O interface. Data acquisition and analysis are performed using software developed in-house (Tofma). With a 233 MHz computer, data can be transferred at rates up to about 300,000 counts per second, limited by the TDC interface hardware. Higher rates may be possible with a more recent version of the TDC, which will have serial Hotlink interface available. Significantly higher data rates can also be obtained using histogramming memory in the TDC.

b) Centaur:

The orthogonal-injection MALDI time-of-flight mass spectrometer (Sciex prototype Centaur) is essentially identical to the MALDI-QqTOF spectrometer described earlier (see Fig. 2-1). The Centaur spectrometer operates at 8 kV acceleration voltage in the TOF section.

Two lasers operating at different wavelength were used to study fragmentation and adduct formation with the Centaur:

1. A nitrogen laser (VSL- 337ND, Laser Science Inc.) operating at wavelength of 337 nm that produced an energy per pulse of approximately 250 μJ was used to irradiate the sample. The laser was coupled to a 200 μm diameter optical fiber by

a 75 mm focal-length lens. The output of the fiber was focused by two 50 mm focal-length lenses to form an image of area ~0.3 $mm^2$ on the target.

2. A Nd-YAG laser (JDS-Uniphase, PowerChip), operating in tripled frequency mode and producing 20 μJ per pulse at the wavelength of 355 nm, was used to generate MALDI ions. A repetition rate up to two kHz is available with this laser, but it produces much smaller energy per shot than the nitrogen laser so the beam must be focused down to a smaller spot size in order to achieve a suitable fluence for MALDI. This was accomplished with the optics shown in Fig. 2-2. Because of the small diameter of the laser beam (1 mm) a negative 10 mm focal-length lens was used to expand the beam. The virtual image from this lens is imaged onto the fiber with two 75 mm focal-length plano-convex lenses arranged in infinite conjugation. A neutral density filter was placed between them.

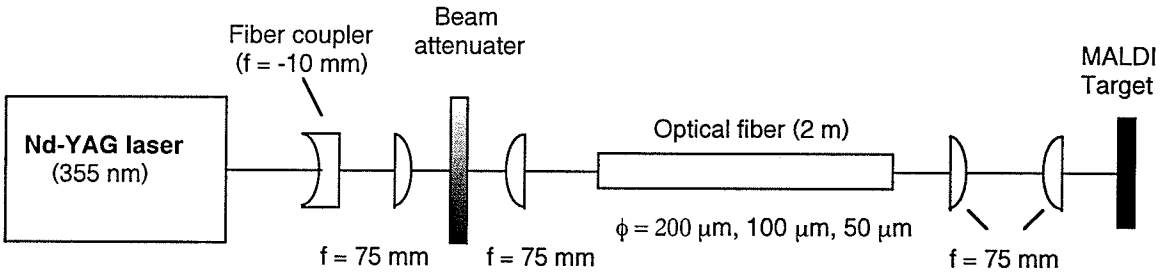


**Figure 2-2.** Fiber-optics setup used to radiate a MALDI target with a beam from an Nd-YAG laser. The beam is directed to an optical fiber using a negative 10 mm focal-length lens. The beam from the fiber is then imaged onto the target by two lenses arranged in infinite conjugation.

The beam was then coupled to optical fibers with diameters of 100 μm, 50 μm or 25 μm. Two 75 mm lens (aberration corrected) were used at the output to image the fiber 1:1 onto the target. The resulting spot size on the target were ~0.053 $mm^3$, ~0.023 $mm^3$ and ~0.016 $mm^3$ for the 100 μm, 50 μm and 25 μm fibers respectively.

The spot size on the target was determined by three components; the fiber diameter ($\phi$), spherical aberration and diffraction all divided by the cos$\theta$ ($\theta$ is the angle to the normal). The spot size due to spherical aberration is equal to $0.067f/f\#^3$ and due to diffraction is equal to $2.44\lambda f\#$, where f# (f-number) is the ratio of the lens' focal length (f) to its clear aperture (effective diameter), and $\lambda$ is the wavelength of the laser beam. The final spot size is calculated by adding the three components in quadrature as shown in Equation 2-1:

$$d = \frac{\sqrt{\phi^2 + \left(\frac{0.067f}{f\#^3}\right)^2 + (2.44\lambda \times f\#)^2}}{\cos\theta} \qquad (2\text{-}1)$$

c) Cone installation

To produce a high-pressure region at the ion source in both instruments a cone with a small orifice was installed between the target and q0, as illustrated in Fig. 2-3. A cone with an orifice ranging from 1 mm to 4 mm in diameter limits the amount of gas flow from one side to the other side. A needle valve was used to vary the amount of gas in the target region. The QqTOF instrument uses a 50 L/s turbo-molecular pump in the q0 region and gas pressures up to 1 Torr can only be achieved. The Centaur spectrometer has a 550 L/s turbo-molecular pump installed in the q0 region which provides the flexibility of maintaining gas pressures ranging from 10 mTorr up to ~3 Torr. The target pressure in the Centaur was monitored by a capacitance diaphragm vacuum gauge (Leybold inficon, model CR090) installed near the source. Spacers of various thicknesses, installed in the Centaur instrument, allow the cone to be located at different distances from the target.

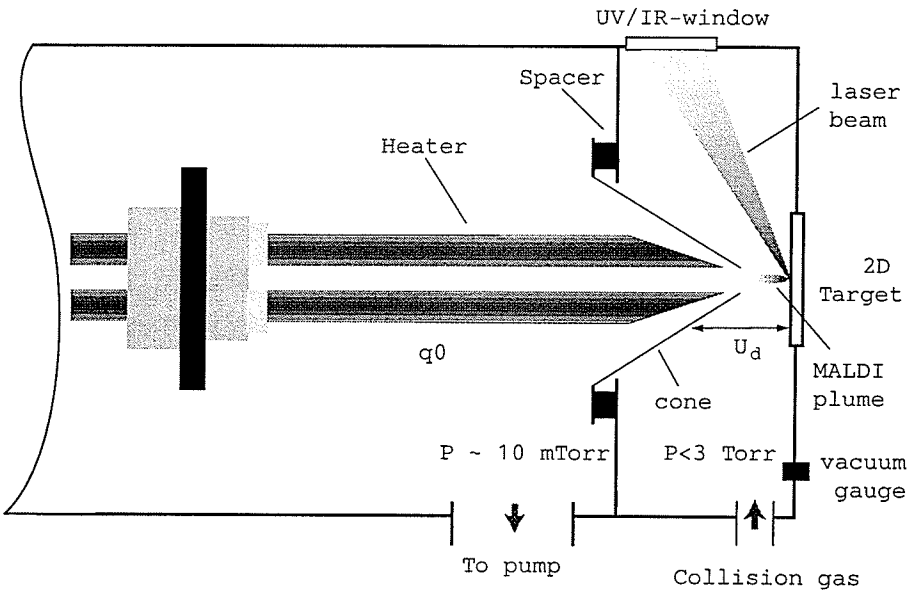


**Figure 2-3.** Schematic diagram of the source region of the Centaur/QqTOF spectrometer. A cone was use to increase the pressure near the MALDI target up to ~3 Torr. Spacers of various thickness allow the cone to be located at different distances from the target.

d) Sample preparation

All peptides and proteins were purchased from Sigma and used without purification. They were dissolved in 5% formic acid in water/methanol (1/1). For MALDI matrices, 2,5-Dehydroxybenzoic (DHB) acid (Sigma) matrix solution (160 mg/ml) was prepared in deionized water/acetonitrile (3/1), and a saturated solution of Alpha-cyano 4-hydroxycinnamic acid (Sigma) was prepared in deionized water/acetonitrile/acetone (3/1/1). Typically, 0.5 – 1 μL of the matrix solution was deposited onto the target spot followed by 0.5-1 μL of the sample solution.

## 2.3 Results

a) High *m/z*:

The performance of orthogonal-injection MALDI TOF spectrometer was explored in MS mode for higher *m/z* using a series of proteins of various masses. The sensitivity begins to decrease rapidly above *m/z* ~ 20,000 because of the low acceleration voltage (8-10 kV), and also because of reduced transmission of large molecular ions through the quadrupole section. Even so, the instrument is capable of analyzing proteins with molecular mass up to about 80 kDa at reduced efficiency, as shown in Fig. 2-4.

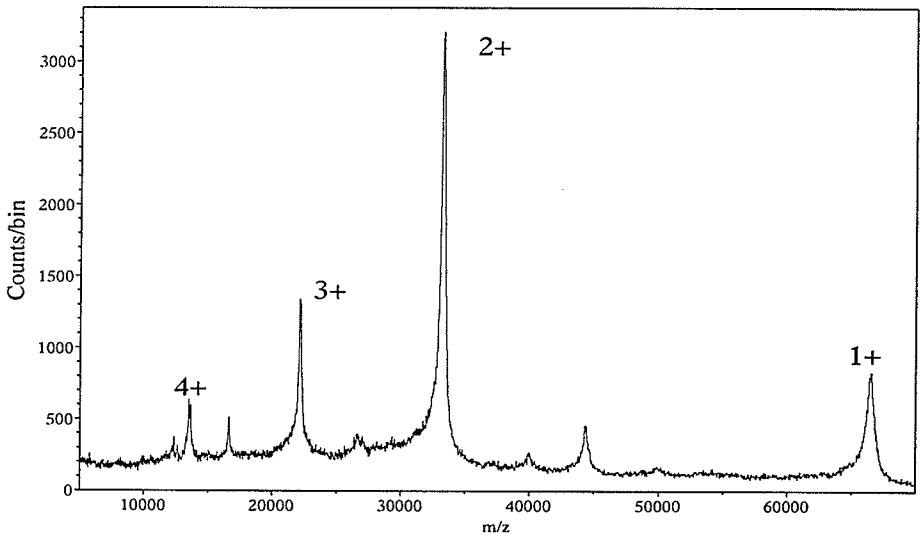


**Figure 2-4.** Positive ion spectrum of bovine serum albumin using DHB as the matrix. The spectrum was recorded in about 10 minutes using a 20 Hz nitrogen laser. It is plotted in 64 ns bins.

A more fundamental problem in analyzing high molecular mass ions in this geometry is metastable fragmentation, that is a loss of $NH_3$ [MH – 17]+ or multiple $NH_3$ or water, in the q0 region, which presumably occurs during the transition interval between desorption/ionization of the sample material and complete cooling of the internal degrees of freedom of the desorbed ions. This time interval is close to the time required

for the ion to reach thermal velocities, which is related to the pressure of the buffer gas. At a pressure of about 10 mTorr in q0 the interval can be estimated to be ~100 μs [5,6].

b) Pressure and cone geometry:

The metastable fragmentation at 10 mTorr produces tails on higher *m/z* peaks and limits the quality of the spectrum, as shown in Fig. 2-4. In fact, under the conditions used to obtain the data of Fig. 2-4, the quality of the spectra of proteins above about 20 kDa, is not better than can be obtained using a simple linear TOF system with delayed extraction. We have therefore attempted to reduce fragmentation by increasing the pressure of the cooling gas in the immediate vicinity of the target. The ion source was modified by placing a cone with a 1.9 mm diameter orifice between the MALDI target and q0, as shown in Fig. 2-3.

With this geometry (1.9 mm cone), the pressure in the ionization region can be increased up to about 1 Torr without increasing the pressure in the q0 ion guide. The increased pressure results in significantly reduced fragmentation for myoglobin, even with the hot matrix α-CHC, as shown in Fig. 2-5c, where the indicated resolving power of 2000 is limited by the pattern of unresolved isotopes. Softer desorption has also been observed for peptides containing oxidized methionine, which usually show a peak corresponding to the loss of $CH_4SO$ (64 Da) that has an intensity comparable to that of the molecular ion. This fragment peak almost disappears when desorption occurs at elevated pressure near 1 Torr.

Further efforts were made to reduce the fragmentation by increasing the target pressure up to 2.5 Torr. This was accomplished by using a cone with a 2 mm diameter orifice and a larger pump in the q0 region on the Centaur instrument. Fig. 2-6 shows the

results of a set of experiments performed at various ion source pressures. The arrow points out the position of the peak corresponding to the loss of $NH_3$ fragment at 0.5 Torr and 2.5 Torr, respectively. In the latter case, the peak has essentially disappeared.

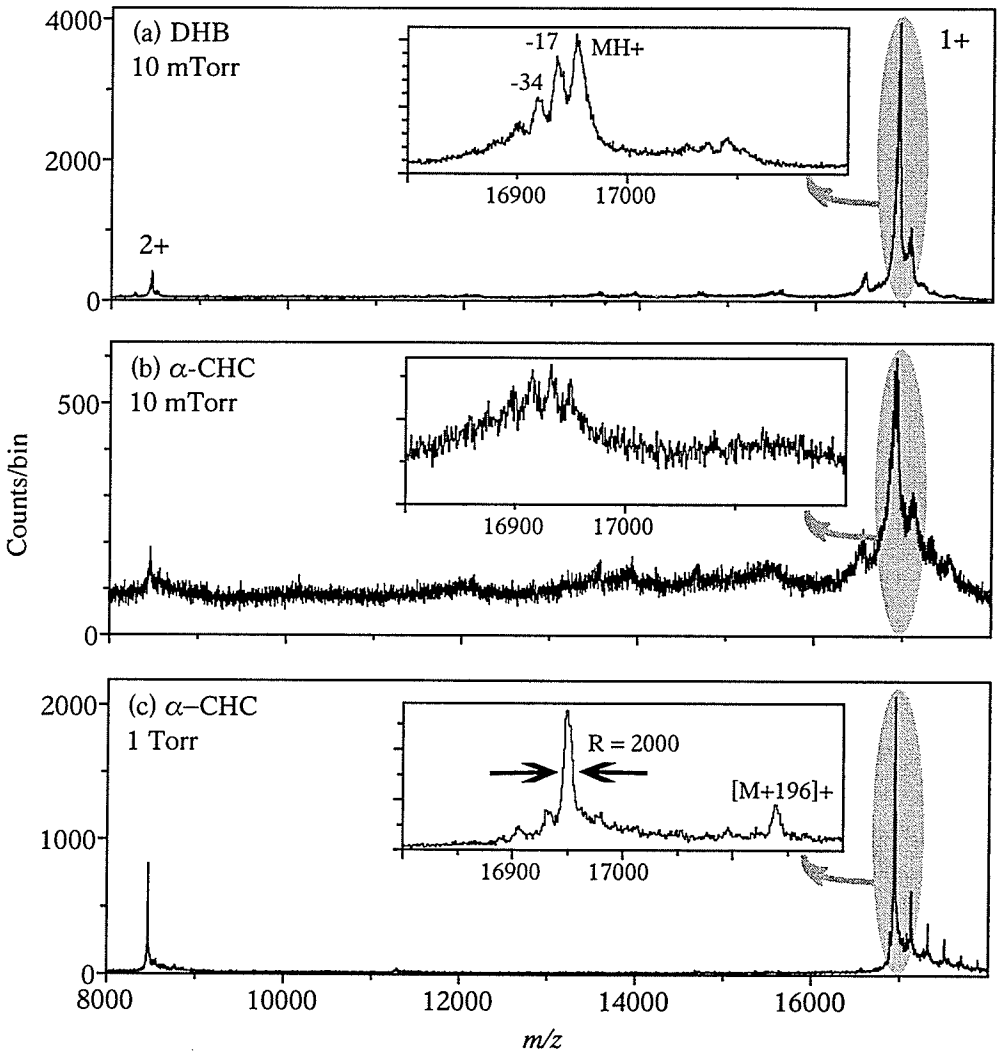


**Figure 2-5.** Positive ion spectra of porcine myoglobin. The spectra in panels (a) and (b) were taken with the pressure near the source the same as in q0 (~10 mTorr); the spectrum in panel (c) was taken at about 1 Torr pressure in the sample chamber. DHB was used as the matrix for spectrum (a); a-CHC was used for (b) and (c). Here the molecular ion peak of myoglobin obtained using 2,5 dehydroxybenzoic acid (DHB) as matrix has two satellites attributed to the loss of $NH_3$, [MH – 17]+ and [MH – 34]+. Matrices characterized as "hot" like α-CHC, produce a higher level of metastable fragmentation (Fig. 2-5b) than do "cold" matrices like DHB.

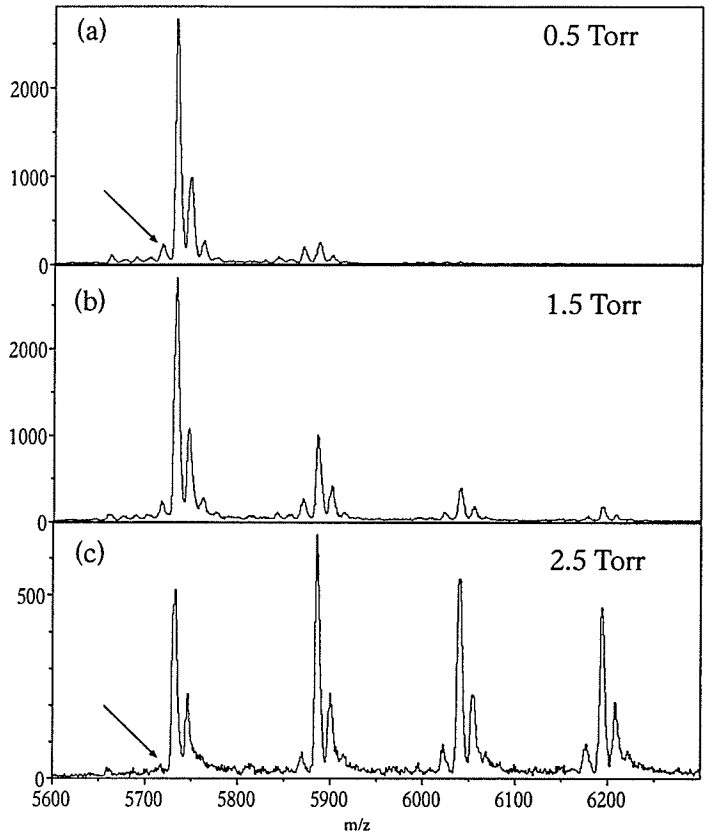


**Figure 2-6**. Mass spectra of insulin with DHB matrix obtained using a 2 mm cone. The sequence of the spectrum demonstrates a gradual reduction and elimination of the $NH_3$ fragment with the increase of pressure at the ion source.

The higher pressure results in increased formation of matrix adducts observed in the spectrum for myoglobin in Fig. 2-5c. For higher *m/z*, such adducts produce tails on the high-mass side much like fragmentation produces tails on the low mass side, and similarly limit spectral quality. It was found that the degree of adduct formation during the expansion of the plume strongly depends on the pressure of the buffer gas at the ion source. Fig. 2-7 shows that the number of matrix adducts attached to the molecule increases with increasing pressure. In this experiment, DHB matrix, MW 154 Da, was used with myoglobin protein. At 600 mTorr ions with at most three matrix adducts are apparent in the spectrum, but at 1 Torr up to 20 (only half are shown) matrix molecules are attached to the protein. Similar results were observed for ferulic, sinapinic and alpha-cyano matrices. For comparable conditions, alpha-cyano matrix has the smallest tendency

to produce adducts, followed by DHB. Ferulic and sinapinic matrices produce similar amount, but noticeably more than DHB.

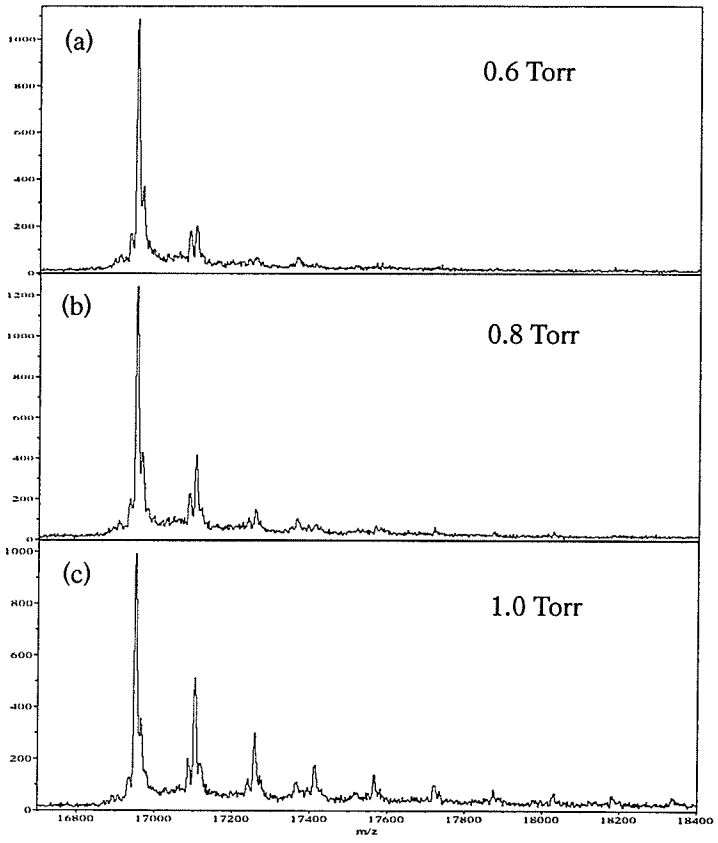


**Figure 2-7**. Spectra of myoglobin with DHB matrix at various buffer gas pressures at the ion source obtained with a 2 mm cone. Higher pressure produces more matrix adducts.

It is important to emphasize that the pressure is measured several cm from the target as a reference, so the exact pressure at the sample surface is not known. Because the cone orifice is near the target there is a strong pressure gradient, so the degree of adduct formation also depends strongly on the spacing between the target and the cone. This spacing also affects the time the ions spend at higher pressure, and the gas flow near the target. For example, an increase as small as 2 mm produces similar number and intensity of adducts as a 0.6 Torr measured pressure increase. The spacing for the experiments of Figs. 2-6 and 2-7 is not known accurately, but was approximately 2 mm.

One limiting factor in using a cone is a decrease in the overall count rate for ions of all masses. The count rate dropped by a factor of three when using a 4 mm cone as compared to no cone, with 10 mTorr at the ion source. However, a substantial increase in the number of ions was obtained when the pressure at the target was increased to 1 Torr; this is due to an improved transmission of the ions embedded in the gas flow. Use of cones with smaller diameter further reduces the count rate; a cone with 1 mm in diameter orifice produced almost no results due to the small number of ions passing through the orifice.

c) Declustering:

The degree of adduct formation can be reduced to some extent, as shown in Fig. 2-8, by increasing declustering voltage ($U_d$) depicted in Fig. 2-3, between the target and the sampling cone to about 40 V. The overall count rate for all mass ions was also improved when a larger declustering voltage was applied.

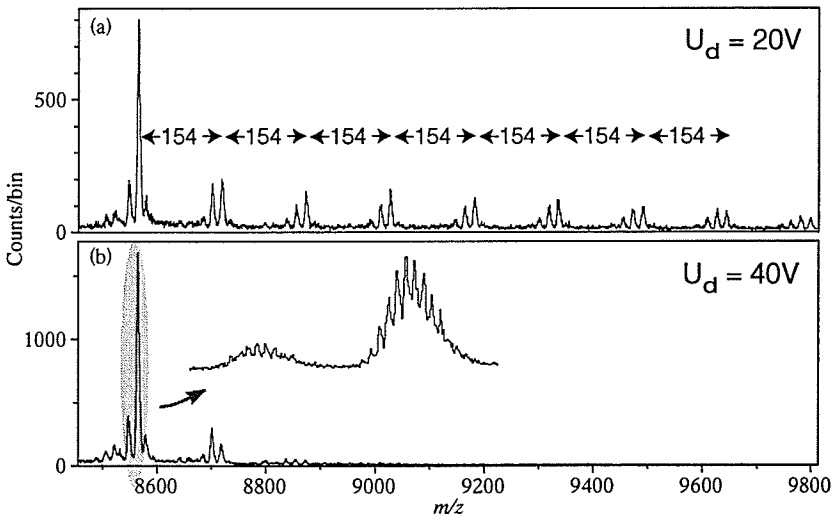


**Figure 2-8.** Spectra of ubiquitin with DHB matrix taken with elevated pressure (~1Torr) near the source, with (a) 20 V and (b) 40 V declustering voltage between the target and the skimmer.

d) Heater

Matrix molecules that attach to proteins and peptides at room temperature can be substantially removed by increasing the buffer gas temperature, see Verentchikov *et al.*

[1]. The temperature of the gas in q0 was controlled using a heater wound around the ion guide as shown in Fig. 2-9. A series of *m/z* mass spectra of ubiquitin with DHB as a matrix obtained at buffer gas temperatures 25 °C, 65 °C and 210 °C is presented in Fig. 2-10. The first spectrum obtained at room temperature has at least 12 DHB molecules attach to the protein. However, more than 80% of adducts detach when the temperature of the collisional cooling gas was increased by 185 °C.

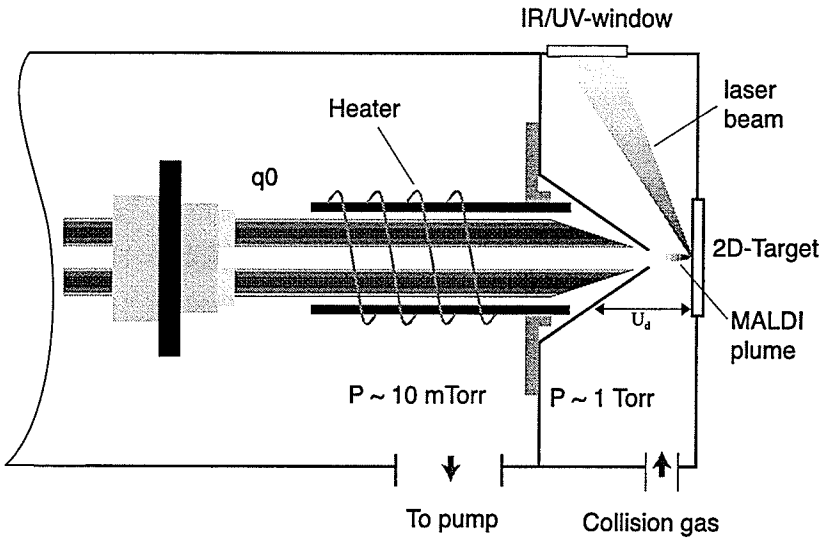


**Figure 2-9**. Schematic diagram of the source region of the QqTOF with a heater to increase the temperature of the buffer gas up to 225 °C.

Figure 2-11 shows overlaid spectra of the doubly charged molecular ion of bovine serum albumin (BSA) obtained at elevated pressure of 1 Torr and at gas temperatures of 24 °C and 225 °C. The full width at half maximum (FWHM) has decreased by 110 Da at higher temperature. It is clearly visible that the tail on the high *m/z* side of the peak produced by matrix adducts has been substantially reduced at 225 °C. The temperature is limited at present to 225 °C by the materials used in the ion source. One can speculate that even higher temperatures will improve the resolution further.

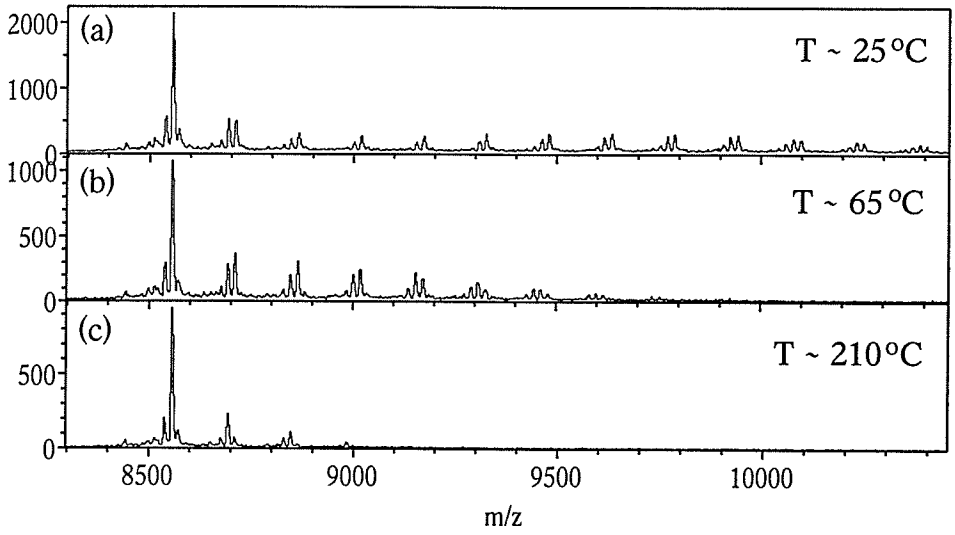


**Figure 2-10.** A sequence of mass spectra of ubiquitin with DHB matrix obtained with the buffer gas temperature at 25 °C, 65 °C and 210 °C. The number of DHB matrix adducts is substantially reduced with buffer gas at 210 °C as compared to room temperature.

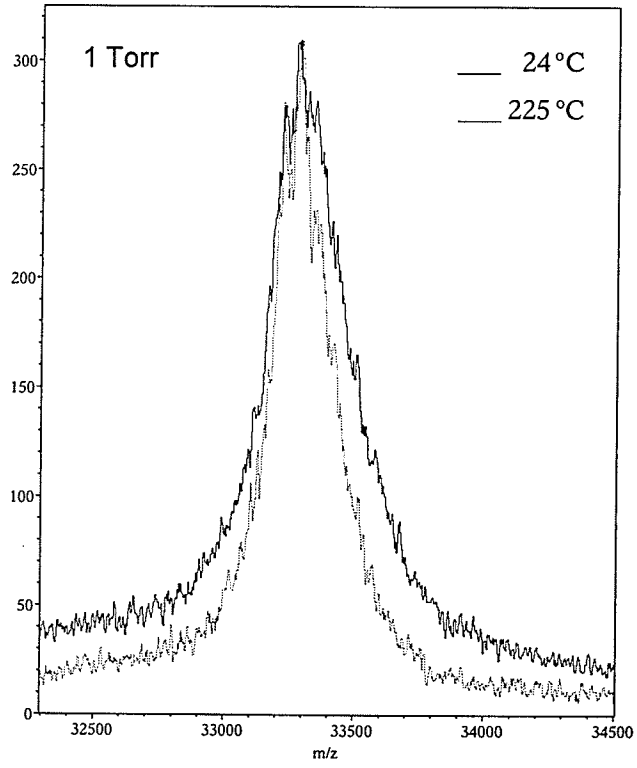


**Figure 2-11.** Overlay of two BSA 2+ spectra at different cooling gas temperatures. The FWHM has decreased by about 110 Da with the increased temperature of the gas. All spectra were taken with the pressure at the target set to 1 Torr.

e) Laser wavelength:

Two lasers operating at wavelengths of 337 nm and 355 nm with pulse width of 4 ns and 0.5 ns respectively were used to investigate the effect of laser conditions on adduct formation and fragmentation. Surprisingly, little or no effect of laser wavelength and pulse width over a small range was observed, as shown in Fig. 2-12. The number of adducts and their relative intensities were found to be comparable for both wavelengths; see Fig. 2-12 which is of insulin with alpha-cyano matrix. The experiment was performed at the same target pressure with a cone of 2 mm orifice. The energy from the $N_2$ laser was approximately 0.2 μJ greater than from the power chip, resulting in slightly greater adduct formation shown in Fig. 2-12(b).

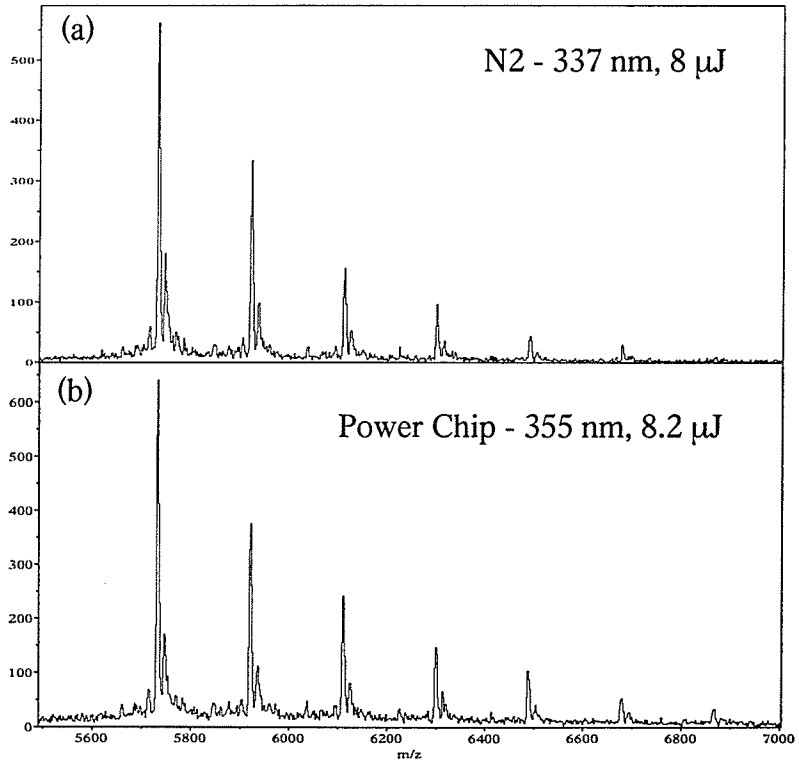


**Figure 2-12.** Mass spectra of insulin with alpha-cyano matrix obtained with N2 laser (a) and power chip laser (b). Both spectra were acquired for about 40 seconds at the same pressure of 2.1 Torr and comparable fluence.

f) Dependence on laser pulse energy:

To measure the effect of laser pulse energy on the mass spectrum, the 200 μm fiber was used with a 4 mm orifice, at a pressure of 0.75 Torr. Fig. 2-13 shows a comparison of three myoglobin spectra with DHB matrix obtained at 16.5 μJ, 21.0 μJ and 26.8 μJ of energy measured at the exit of the fiber. For increasing energy, the main effect is that adduct formation becomes much more prominent. The degree of fragmentation also increases slightly. Similar result applies to lighter proteins and peptides.

Furthermore, the formation of matrix adducts was studied by radiating the sample at different energies using 200 μm and 50 μm fibers. With the 200 μm fiber the laser energy was set to 12.7 μJ and 8.5 μJ, as measured at the output of the fiber. The result shown in Fig. 2-14, demonstrates that significantly more matrix molecules attach to the analyte ion at larger laser energy. With the 50 μm fiber the energy was adjusted to 3 μJ and 1.7 μJ (measured at the output of the fiber). Fig. 2-15 shows the results obtained at the two different laser energy settings. It is apparent that only one matrix molecule was formed in the spectrum 2-15 (b) as compared to six adducts found in spectrum 2-15 (a). This result demonstrates that matrix adducts can be dramatically suppressed with a 50 μm fiber and low laser energy, while still using a high pressure to suppress fragmentation. However, the number of ions produced at this condition is substantially lower.

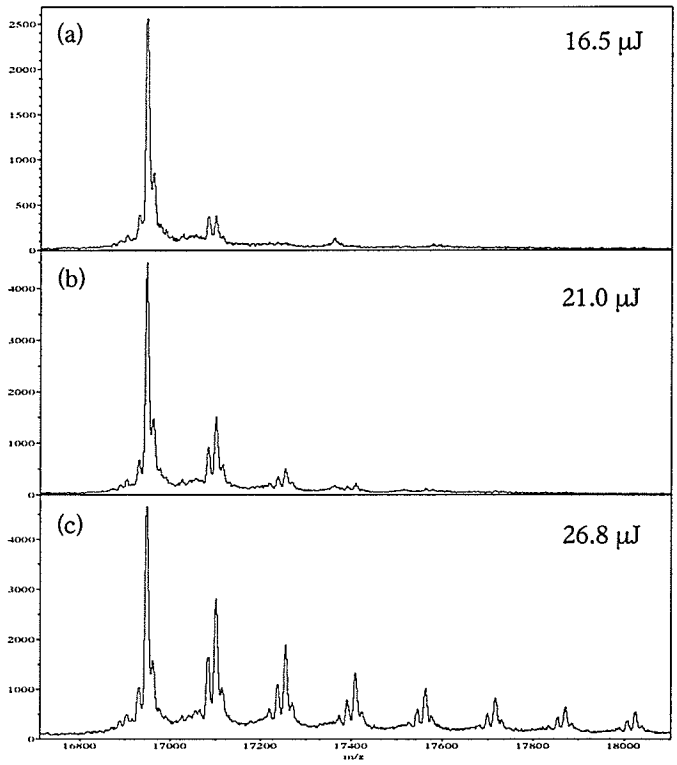


**Figure 2-13.** Mass spectra of myoglobin with DHB matrix obtained at 16.5 μJ (a), 21.0 μJ (b) and 26.8 μJ (c) of laser energy. All spectra were obtained at 0.75 Torr of pressure using a 4 mm orifice.

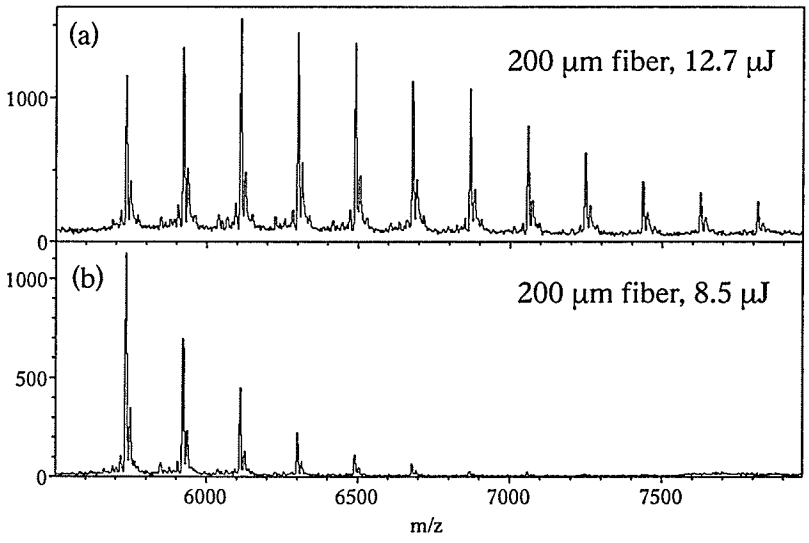


**Figure 2-14.** Mass spectrum of insulin using alpha-cyano as matrix. The spectra were obtained using a 200 μm fiber with a laser energy set to 12.7 μJ (a) and to 8.5 μJ (b). Substantially more matrix adducts are observed at higher laser energy.

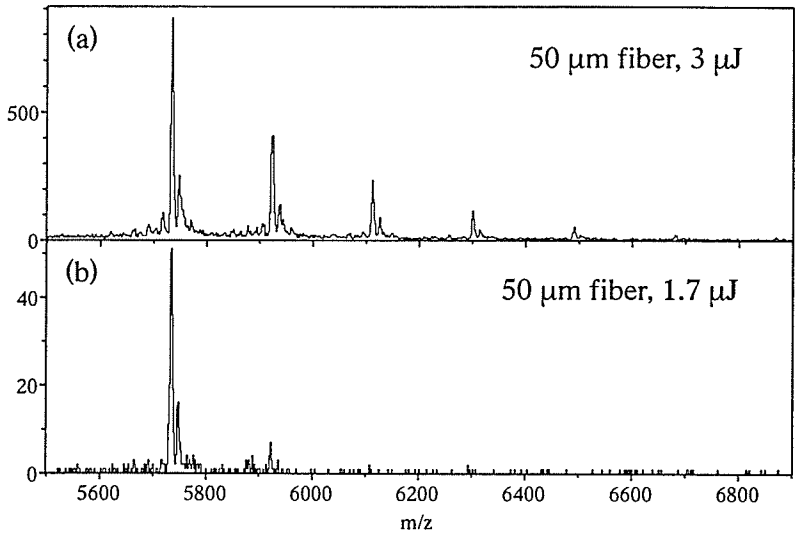


**Figure 2-15.** Mass spectrum of insulin using alpha-cyano as matrix. The spectra were obtained using a 50 μm fiber with a laser energy set to 3 μJ (a) and to 1.7 μJ (b). More matrix adducts are observed at larger laser energy.

g) Spot size:

Adduct formation produced during the MALDI process at 2.1 Torr of nitrogen gas was investigated with three different spot sizes produced using fibers of three different diameters. The beam was transmitted through three fibers (200 μm, 100 μm and 50 μm) and ideally imaged 1:1 on the target. However, due to optical aberrations introduces by spherical lenses the spot sizes were actually equivalent to circular spots with diameters of about 330 μm, 190 μm and 130 μm for the 200 μm, 100 μm and 50 μm fibers, respectively. To isolate the effect of the spot size, it was decided to keep the (total counts over a particular mass range) divided by (image spot size) a constant. This presumably reflects similar plume density, and comparable sample usage in practical situations. The alternative – to keep the laser fluence constant – was difficult because the aberrations play more significant role in power distribution across the small spot, moreover according to [7] the count rate decreases with decreasing spot size much faster than linear. To get a constant value, the fluence (energy per unit area) was adjusted to 260

J/m$^2$, 450 J/m$^2$ and 610 J/m$^2$ for the 200 μm, 100 μm and 50 μm fiber, respectively. We found that experiments performed with the 200 μm fiber produced the largest number of adducts, as illustrated in Fig. 2-16.

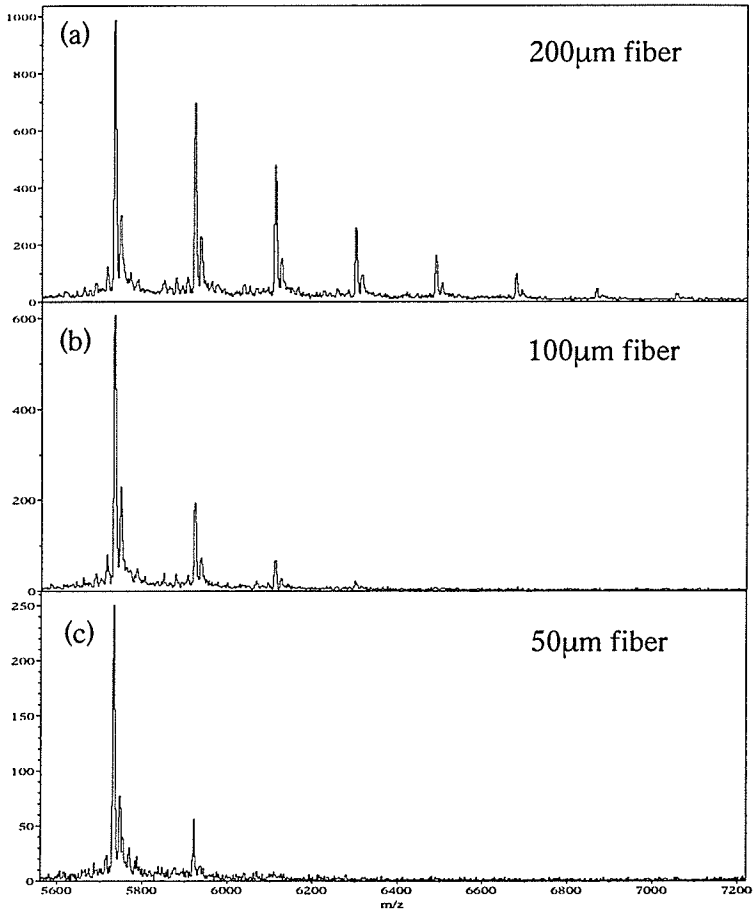


**Figure 2-16.** Mass spectra of insulin with alpha-cyano matrix obtained with three fibers ranging from 200 μm to 50 μm in diameter. The 200 μm fiber creates more adducts than the 50 μm fiber.

## 2.4 Discussion

Our experiments are consistent with an overall picture where biomolecules survive the vigorous desorption/ionization process in the rapidly expanding plume because of cooling which results from collisions with matrix molecules and buffer gas. The interactions provide cooling of the analyte molecules. Improved cooling is achieved by increasing the

pressure of the buffer gas. At the same time higher pressures produce matrix adducts because of increased interaction between the analyte and the gas molecule. The degree of metastable decay and adduct formation depend on the pressure of the buffer gas, laser pulse energy, and spot size. These various conditions effectively change the pressure near the ion source. Matrix adducts are mainly removed by either declustering voltage or by increasing the buffer gas temperature.

Increased buffer gas pressure (up to 2.5 Torr) at the MALDI ion source dramatically reduces metastable fragmentation of peptides or proteins. The denser buffer gas increases the collision probability of the analyte, and the cooling happens before the metastable decay. During the collisions with buffer gas the analyte loses some of its kinetic energy, which leads to more stable ions and thus less fragmentation of the analyte is observed during acquisition time.

At high *m/z* ratio, matrix adducts produce tails on the high mass side of the peak and spoil mass resolution. The formation of matrix adducts depends on pressure, laser pulse energy and spot size. The larger laser pulse energy and higher source pressure produces a bigger MALDI plume and hence the ions collide and attach to matrix molecules more readily. The results with spot size are also consistent. A large spot size (for the same fluence) should produce a larger plume and therefore less fragmentation and more adducts.

The declustering voltage, which produces larger electric fields between the target and the cone, increases the kinetic energy of the molecules. These higher energy molecules create more energetic collisions with buffer gas and break the weaker molecule-matrix bonds. Similarly, an increased temperature of the buffer gas also

produces more energetic collisions between analyte and buffers gas. A chart identifying the UV-MALDI process at low and high pressures is illustrated below

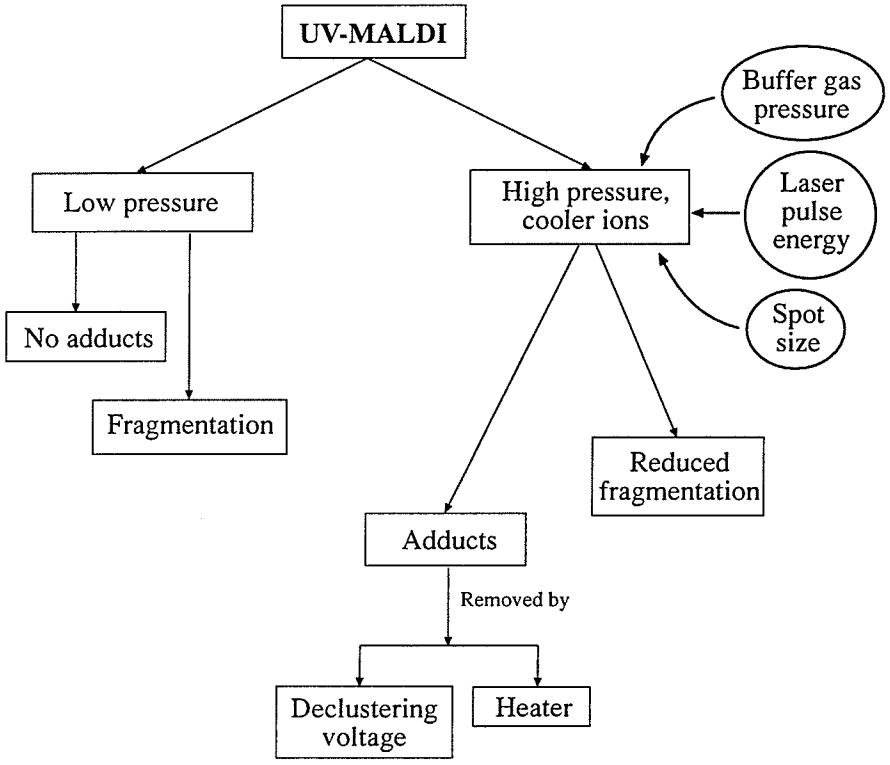


**Chart 1**: A visual representation of the many step UV-MALDI process at low and high pressures at the ion source.

Optimum conditions for peptide (low *m/z*) analysis with DHB matrix are 10 mTorr target pressure (with no cone) and 200 μm fiber. DHB matrix is known to be a cooler matrix [8]. For analysis of peptides with other matrices that produce more fragmentation such as alpha-cyano matrix, better results are obtained at elevated pressures as less fragmentation and greater sensitivity is observed. We found that, for the higher mass range, above 10 kDa, the most desirable condition for low fragmentation and for low adduct formation is obtained with the 50 μm fiber, high pressure (~2 Torr) and low laser energy setting. However, the ion count rate produced at this condition is substantially smaller as compared to the count rate produced at normal conditions; 200

μm fiber with the ion source at 10 mTorr. We speculate that the small count rate created by the small fiber setting can be compensated with a higher repetition rate laser.

## 2.5 Conclusion

We have shown that by increasing the pressure of the buffer gas from 10 mTorr up to ~3 Torr near the ion source using a cone with a small orifice can significantly reduce the metastable fragmentation of peptides and proteins occurring in the q0 region.

The elevated pressure near the target produces matrix adducts that attach to precursor ions. Matrix adducts appear on the right hand side of the peak and at high *m/z* produce tails that strongly decrease the performance, including sensitivity and mass accuracy of the orthogonal MALDI TOF-MS. The number and intensity of matrix adducts strongly depend on laser energy, pressure and spot size.

Fortunately, the matrix adducts are partially eliminated by either increasing the voltage between the target and the cone or by increasing the temperature of the buffer gas from room temperature up to +210 °C.

# CHAPTER 3

## Orthogonal-injection MALDI with an infrared laser; optimizing oMALDI conditions for analysis of DNA

### 3.1 Introduction

The axial geometry is readily used with UV and sometimes infrared-MALDI ion source. The UV-MALDI ion source in axial geometry is normally used for the analysis of peptides and proteins and sometimes DNA and RNA. However, the mass accuracy and resolution obtained for the heavier molecules (>20 kDa) is poor. This is due the metastable fragmentation of proteins and base-loss of DNA/RNA in the drift region or during acceleration which produces peak broadening, as explained in Chapter 2. In the axial geometry, even for low mass where high performance is possible with UV MALDI, it requires considerable effort in optimizing sample preparation, type of matrix and laser fluence.

Previous experiments have shown that infrared (IR) excitation produces cooler ions; meaning reduced metastable fragmentation, and an increased mass range. Berkenkamp *et al.* have shown mass spectra of DNA up to mass 673 kDa obtained with IR-MALDI in reflecting geometry [1]. Unfortunately an IR laser introduces matrix adducts that produce high mass tails and once again spoil mass resolution [2]. Moreover, some IR lasers produce light pulses with pulse widths that are two orders of magnitude larger than the typical pulse width produced by UV lasers. The long pulse width and the typically employed glycerol liquid matrix in IR-MALDI further decrease the mass resolution and accuracy in axial instruments for the entire mass range. This is particularly true in the high mass range where for the large DNA spectrum just mentioned the mass resolution is only about 70 [1].

In orthogonal MALDI, the decoupled ion source allows greater flexibility to vary the target conditions, such as ionization conditions, sample charging or target irregularities without affecting the performance of the instrument. Moreover, the decoupled ion source allows the use of lasers with long pulse lengths without spoiling mass accuracy and resolution.

In this chapter we report the very first experiments with an IR-MALDI ion source on the orthogonal-injection TOF mass spectrometer. We present some related investigations of the problems encountered in the analysis of DNA with both UV and IR MALDI.

## 3.2 Experimental

a) Instrumentation:

All mass spectra were obtained using a QqTOF mass spectrometer. The schematic diagram of the orthogonal-MALDI TOF is shown in Chapter 2. For UV-MALDI the standard $N_2$-laser was used with the same optical setup as described in the previous chapter.

A 2.94 μm Q-switched Er:YAG laser (model Bioscope IR laser Probe, Bioptics) with a 150 ns pulse width and a maximum energy of 15 mJ was used for IR-MALDI. A 25 mm plano-concave lens and a 10 mm plano-convex sapphire lens were used to focus the beam to a spot size of about 250 μm in diameter. The laser beam was attenuated using two 1.3 mm thick microscope slides.

To reduce metastable fragmentation of proteins and base-loss of DNA the pressure of the buffer gas near the target was increased to 1 Torr using a cone with a 1.9 mm diameter orifice, positioned between the MALDI 2D-target and the collisional ion guide (see Chapter 2 for more detailed discussion). To reduce the problem of adduct formation, the temperature of the buffer gas was increased from room temperature up to +225°C using a resistive heater wound around the ion guide, see Chapter 2 Fig. 2-3.

A special target equipped with a Peltier element was used to freeze a water matrix and to cool glycerol matrix down to –25 °C. The schematic and photo of the target is shown in Fig. 3-1.

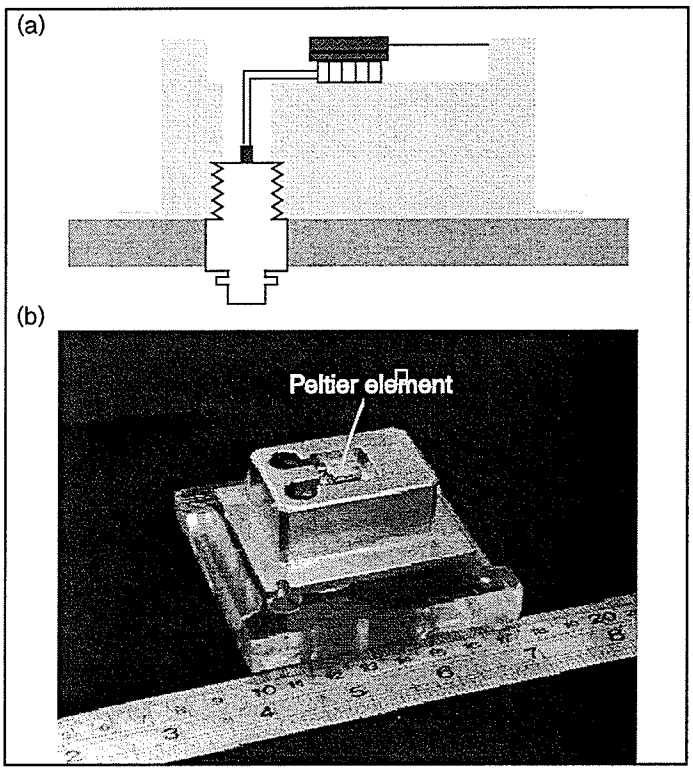


**Figure 3-1.** (a) Schematic diagram of QqTOF 2-D target with Peltier element used to freeze samples. (b) Photograph of the 2-D target with Peltier element.

b) Sample preparation:

All proteins and peptides, purchased from Sigma, were prepared using aqueous 0.1% TFA to a desired concentration. UV-MALDI matrices, 2,5-dihydroxybenzoic (DHB) acid (from Sigma) matrix solution (100 mg/mL) and saturated solution of alpha-cyano-4-hydroxycinnamic acid (from Sigma) were prepared in water/acetonitrile (2:1 vv). 3-hydro-pycolinic acid (3-HPA) used for study of DNA in UV-MALDI was prepared by a similar method as the matrices.

DNA samples were obtained from Metabion (Germany). DNA stock solutions

were prepared to 100 pmol/μL with deionized/nanopure water and then diluted as required. The two matrices used for IR-MALDI were glycerol (Alfa Aesar) and saturated solution of succinic acid in deionized water. Ion exchange beads, DOWEX-50W, were used for desalting glycerol matrix.

Normally, a small drop of glycerol was first deposited on the target followed by 0.5 – 1 μL of the analyte and then approximately 0.5 μL of the ion exchange beads was added on top of the glycerol/analyte mixture. Best results were obtained when the beads were well mixed with the glycerol/analyte mixture and the sample was cooled down to –25 °C.

## 3.3 Results

a) Low mass proteins and DNA

In this section all results were obtained simply by substituting an IR laser for the UV laser in the QqTOF instrument. Thus the data are obtained with the typical operating conditions of the QqTOF instrument [3] (similar to those of the Sciex QStar), without a cone and with 10 mTorr buffer gas pressure.

As expected, the resolution and accuracy of orthogonal MALDI with an infrared laser is very much comparable to UV excitation. Fig. 3-2 shows an IR-MALDI mass spectrum of a mixture of dalargin, substance P and melittin. Resolution of about 10,000 at full-width half maximum (FWHM) is obtained throughout the mass range just as in the UV case, (Fig. 1-7). In contrast to axial MALDI, the width of the IR laser pulse does not cause peak broadening in the low mass range as shown in the figure. The spectrum of the mixture of peptides was obtained using a glycerol matrix.

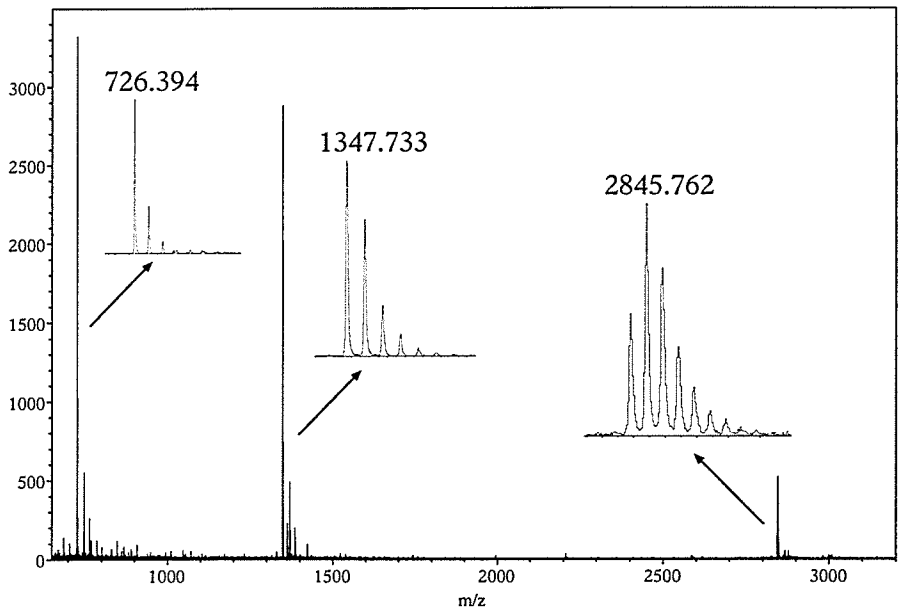


**Figure 3-2.** Positive ion mass spectrum of a mixture of: dalargin, substance P and melittin. The spectrum illustrates a uniform resolution power M/ΔM (FWHM) of about 10,000 throughout the mass range.

IR-MALDI was investigated using DHB, succinic acid, urea and glycerol matrices. Glycerol proved to be the most versatile matrix for both protein and DNA analysis. It worked for a broad mass range with long lasting and strong analyte signal. DHB matrix worked just as well in the low mass range, but was ineffective above 10 kDa. DHB is the preeminent matrix for the analysis of both peptides and proteins in orthogonal UV-MALDI. However, 3-HPA was employed for the study of DNA with UV excitation.

Mass accuracy of approximately 10 ppm is obtained with both IR and UV ion sources when an external 2-point calibration is performed within about 30 minutes of the measurement. Internal calibration allows the mass accuracy to be improved to a few ppm. The mass spectrum in Fig. 3-2 and in every other figure reported here illustrates the true raw data without any smoothing or any other type of enhancement. However, the bin size might vary considerably from spectrum to spectrum.

A mass spectrum of a double-stranded DNA of 12, 20 and 25 bases in length with mass of 3628.8 Da, 6131.0 Da and 7687.2 Da, respectively was easily obtained with both

UV and IR-MALDI. The spectra of these DNA were easily reproducible with a comparable mass resolution (10,000) and mass accuracy (<14 ppm). IR-MALDI mass spectra of the 20 mer and 25 mer DNA are shown in Fig. 3-3.

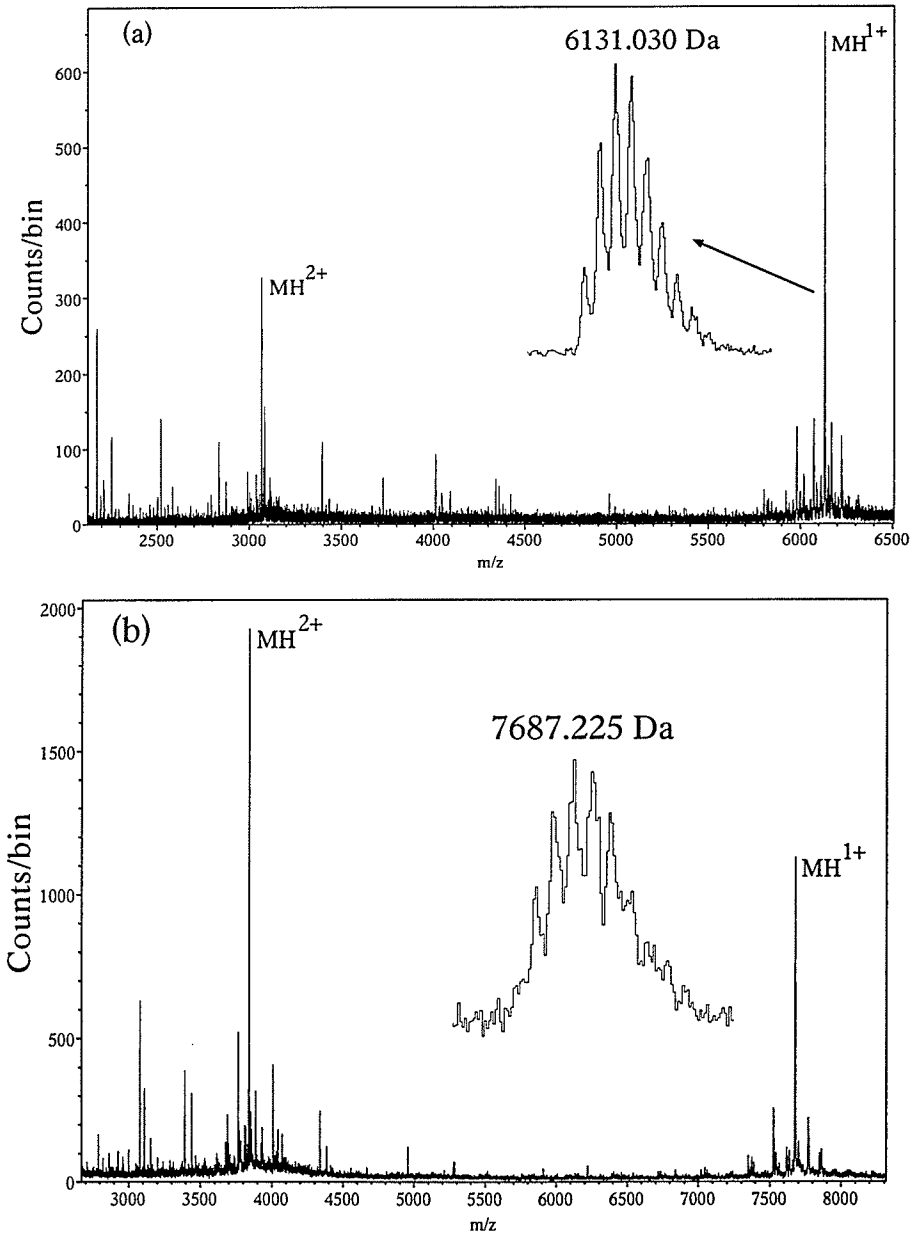


**Figure 3-3.** IR-MALDI spectrum of 20 mer (a) and 25 mer (b) using glycerol as a matrix. The insert illustrates the isotopic mass resolution of ca. 10,000 at *m/z* 6131 Da and 7687 Da for the two DNA.

A good quality MS/MS mass spectrum of a 12 mer DNA has also been obtained using UV and IR-MALDI; the former is shown in Fig. 3-4. The spectrum consists of fragments cleaved at 3-prime end. A table of the calculated mass fragments of individual nucleotides, verses their experimental mass and the differences is shown in Table 1. The accuracy for the fragment ion peaks range from 10 ppm to 50 ppm allowing easy assignment of sequence-specific fragments and indicating potential for direct sequencing of short DNA strands. Only 12 mer DNA was sequencd due to the mass limit of 6000 Da on the quadrupoles. Although all the nucleotides were observed in the UV spectrum, we found three missing nucleotides in IR-MALDI mass spectrum of 12-mer DNA. Once the ions are collisionally cooled to equilibrium, it is seems unlikely that the origin should play a role in the fragmentation, so we are unable to explain this difference.

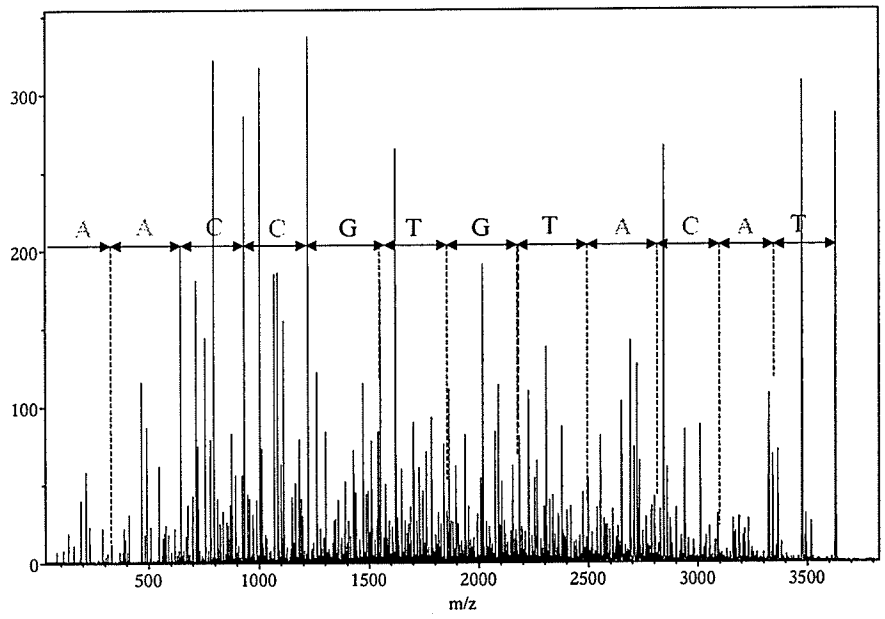


**Figure 3-4.** UV-MALDI tandem mass spectrum of 12 mer DNA. The fragments are cleaved at the 3- prime end.

| Nucleotide | Calculated Mass (Da) | Mass Found (Da) | Δm (Da) |
|---|---|---|---|
| 3' – d(A) | 332.076 | 332.057 | +0.019 |
| 3' – d(AA) | 645.134 | 645.128 | +0.006 |
| 3' – d(AAC) | 934.180 | 934.169 | +0.011 |
| 3' – d(AACC) | 1223.226 | 1223.219 | +0.007 |
| 3' – d(AACCG) | 1552.279 | 1552.222 | +0.057 |
| 3' – d(AACCGT) | 1856.325 | 1856.307 | +0.018 |
| 3' – d(AACCGTG) | 2185.377 | 2185.313 | +0.064 |
| 3' – d(AACCGTGT) | 2489.423 | 2489.486 | -0.063 |
| 3' – d(AACCGTGTA) | 2802.481 | 2802.453 | -0.028 |
| 3' – d(AACCGTGTAC) | 3091.527 | 3091.556 | -0.029 |

**Table 1**: MS/MS fragments of 12 mer DNA of a known sequence 5'-TAG ATG TGC CAA –3'.

Sensitivity in IR-MALDI is considerably poorer than in UV-MALDI, especially for the analysis of DNA. Nevertheless we were able to obtain an IR-MALDI spectrum of BSA (66 kDa) using only 0.5 pmol of sample. With increased amounts (~25 pmol), dimers, trimers and hexamers were observed.

We found that for a 12-mer DNA strand, IR-MALDI consumed five times the amount sample in order for the count rate to be comparable to UV-MALDI. A comparison of 36 mer DNA with UV and IR-MALDI is presented in Fig. 3-5. The mass resolution and mass accuracy in both cases was comparable. However, for UV MALDI (figure a) we see an extensive loss of bases of mass ~151.05 Da present to the left of the parent ion as compared to figure (b).

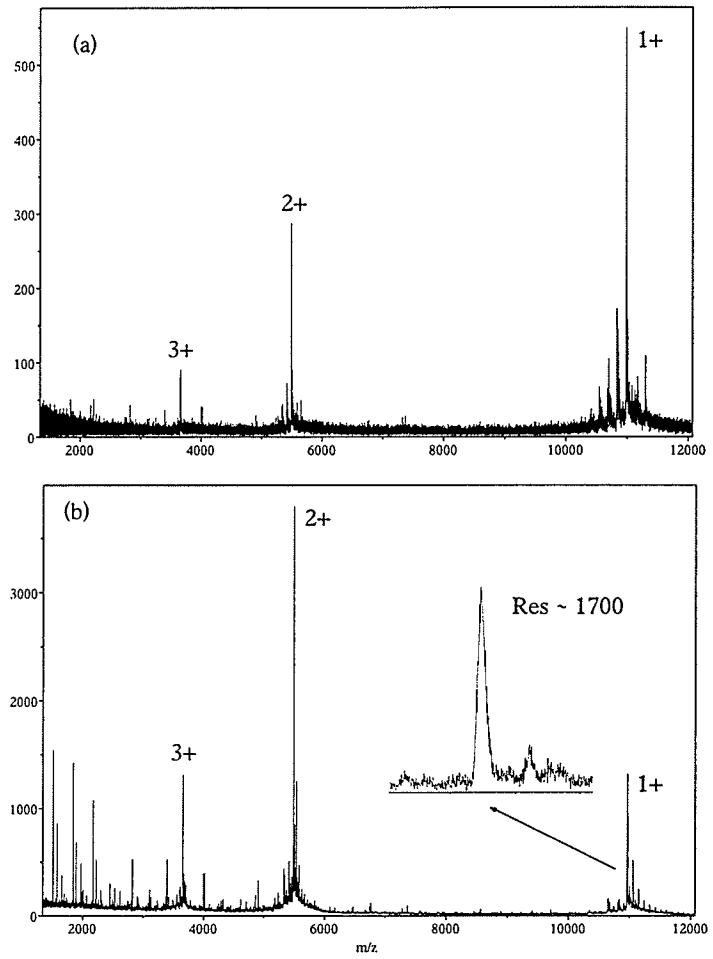


**Figure 3-5.** Mass spectra of 36-mer DNA obtained using (a) UV-MALDI with DHB matrix and (b) IR-MALDI with glycerol matrix.

b) Characteristics of IR and UV-MALDI at higher mass

At higher mass, the effect of using an IR laser with the usual pressure in the source region (~10 mTorr) is similar to using a UV laser with elevated pressure (~1 Torr). That is, the spectra show dramatically reduced metastable fragmentation, but increased adduct formation, as shown in Fig. 3-6.

Increase of the buffer gas pressure at the ion source had no effect on the IR-MALDI spectrum. Fig. 3-7 shows a spectrum of myoglobin obtained at 10 mTorr (a) and 1 Torr (b) of pressure. There is no difference in the fragmentation and degree of adducts formation between the two spectra.

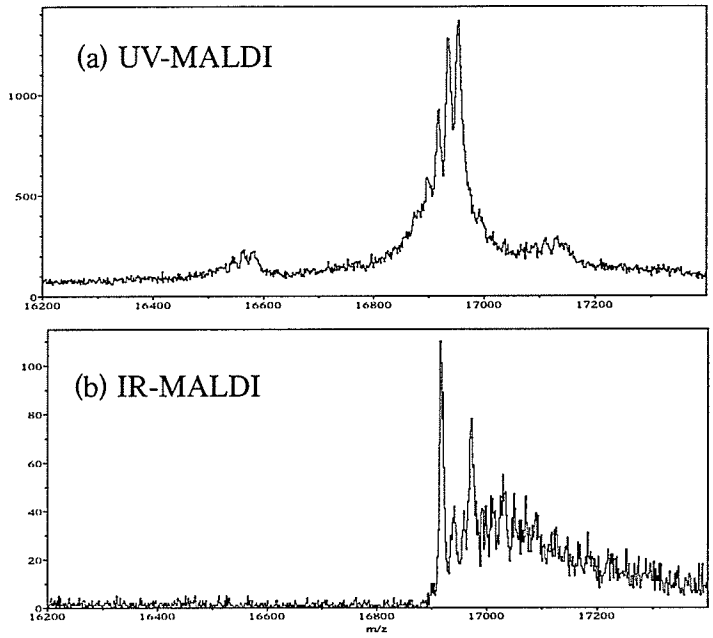


**Figure 3-6.** UV and IR MALDI spectra of horse (a) and sheep (b) myoglobin obtained with the pressure near the ion source set to 10 mTorr.

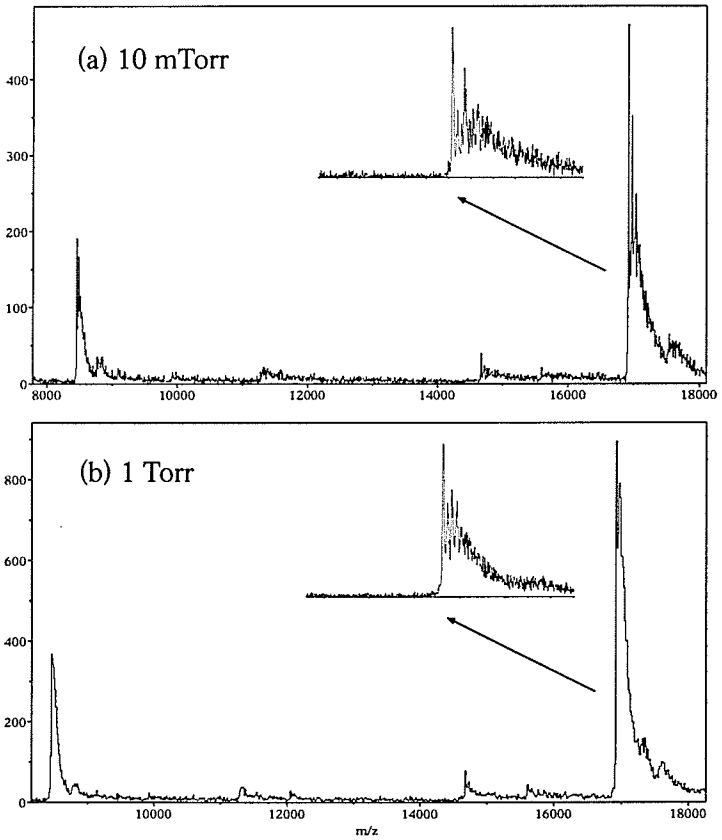


**Figure 3-7.** IR-MALDI spectra of sheep myoglobin from glycerol matrix. The spectrum in panel (a) was taken with the pressure near the target set to 10 mTorr and 1 Torr for panel (b).

Our initial experiments with IR-MALDI using glycerol as a matrix showed serious problems with salt (Na) adducts, which were not susceptible to declustering voltage. Initially, we tried to reduce the effect by using an ultra-clean target surface, but the problem was not completely resolved. Significant progress has been made in reducing the salt and potassium adducts by using ion exchange beads as shown in Fig. 3-8. The ion exchange beads were mixed with the glycerol matrix on a target, in a ratio of 50/50 by volume.

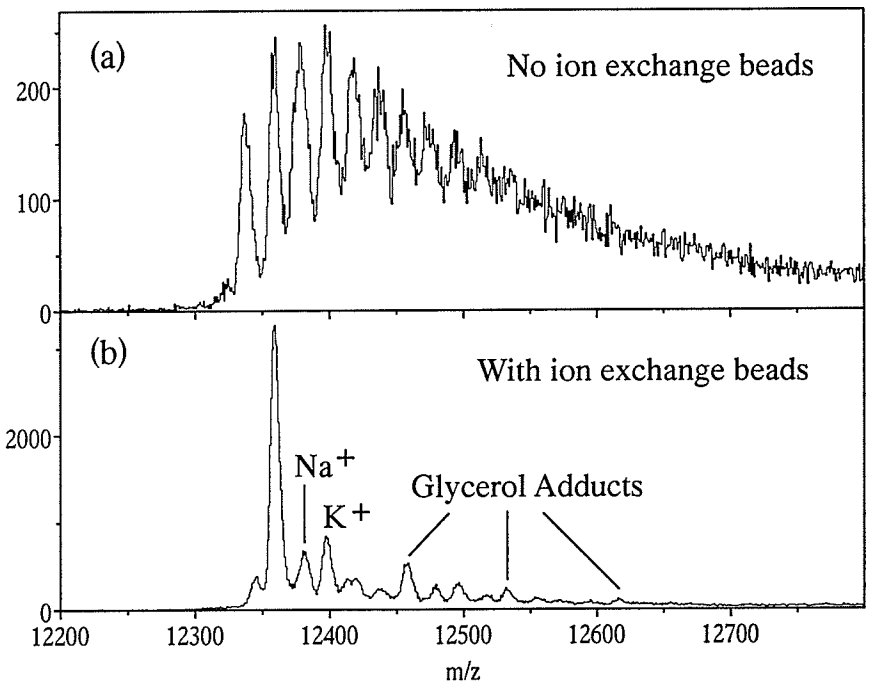


**Figure 3-8.** IR-MALDI mass spectrum of cytochrome C using glycerol as the matrix. The distribution of peaks found to the right of the first peak in (a) consists mainly of Na adducts which are removed by ion exchange beads in (b).

The remaining adducts such as matrix molecules, including glycerol, that attach to proteins and DNA in IR-MALDI, can be substantially removed by increasing the temperature of the buffer gas up to 220 °C. In Fig. 3-9 we see a mass spectrum of 36-mer DNA obtained with glycerol matrix. The first spectrum was acquired at room temperature and six glycerol molecules attach to the DNA. Adducts detached when the temperature of the buffer gas was increased to 200 °C.

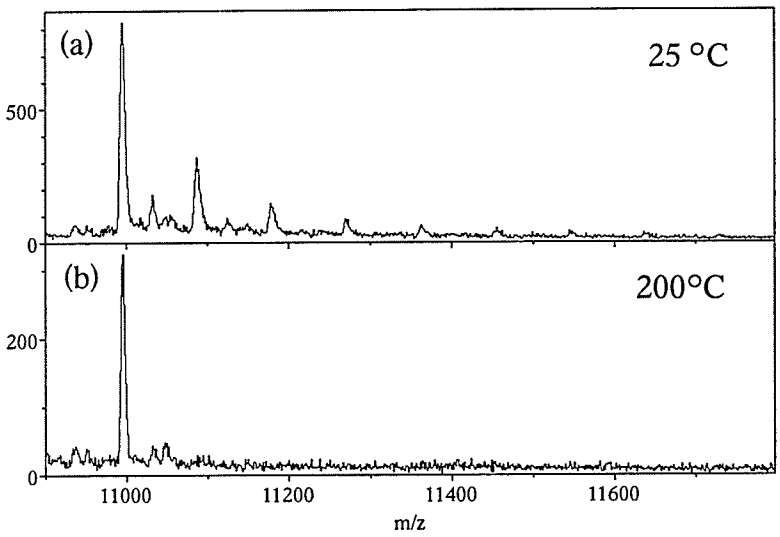


**Figure 3-9**. IR-MALDI mass spectra of 36-mer DNA using glycerol matrix obtained at buffer gas temperature of 25 °C (a) and 200 °C (b).

For proteins like myoglobin or larger, under some conditions at least, IR-MALDI using a glycerol matrix produces much higher charge states than are observed in UV-MALDI in this instrument, see Fig. 3-10. This may be an important advantage because it avoids the practical difficulties of introducing a high accelerating voltage or post-acceleration to obtain acceptable detection efficiency.

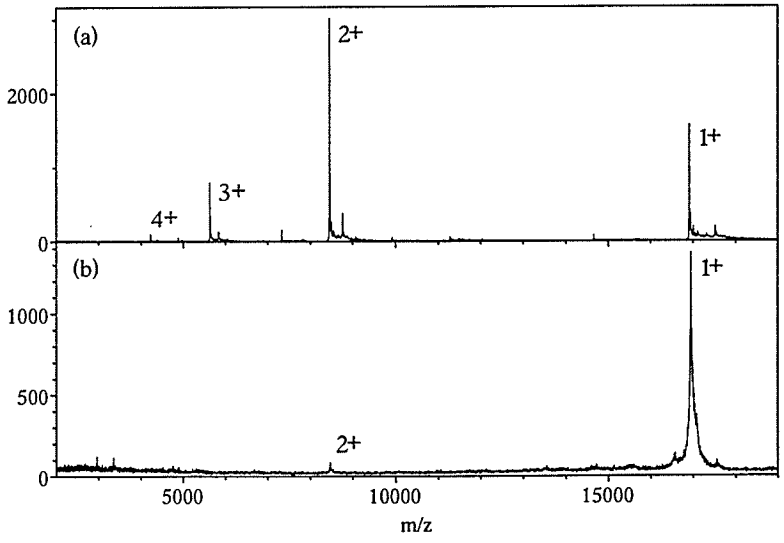


**Figure 3-10**. (a) IR-MALDI and (b) UV-MALDI mass spectrum of sheep myoglobin. Glycerol and DHB matrix were used for IR and UV-MALDI, respectively. The IR

excitation produces higher charge states ions than UV excitation.

c) High mass DNA with UV-MALDI

Although IR seems to provide a softer method of ionization at 10 mTorr, the best results for heavy DNA were obtained with UV-MALDI using a cone to provide high pressure near the target. This is because the UV excitation is much more sensitive to DNA than IR, as mentioned earlier. Fig 3-11 illustrates mass spectra of 36-mer DNA obtained at 10 mTorr (a) and 1 Torr (b). The elevated pressure somewhat reduces the loss of bases of mass ~151.05 Da present to the left of the parent ion.

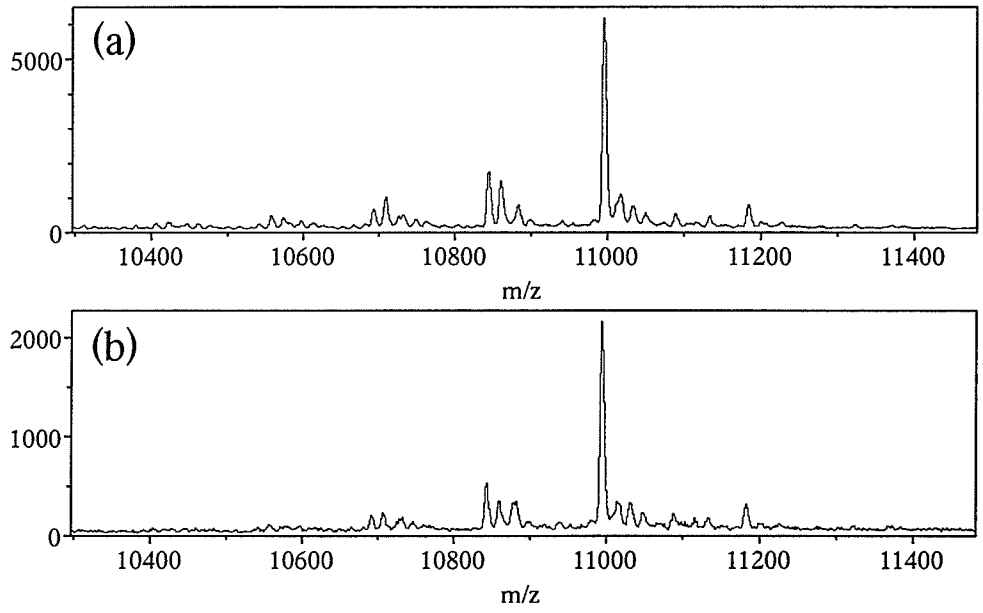


**Figure 3-11.** UV-MALDI mass spectra of 36-mer DNA obtained at 10 mTorr (a) and at 1 Torr (b). The matrix used for this study was 3-HPA.

We found that the best quality mass spectra were achieved when the ion exchange beads were mixed with the aqueous DNA. Fig. 3-12 shows 60-mer DNA obtained with and without the ion exchange beads. The beads dramatically reduce sodium adducts and improved the effective mass resolution from 25 to 2500 (FWHM).

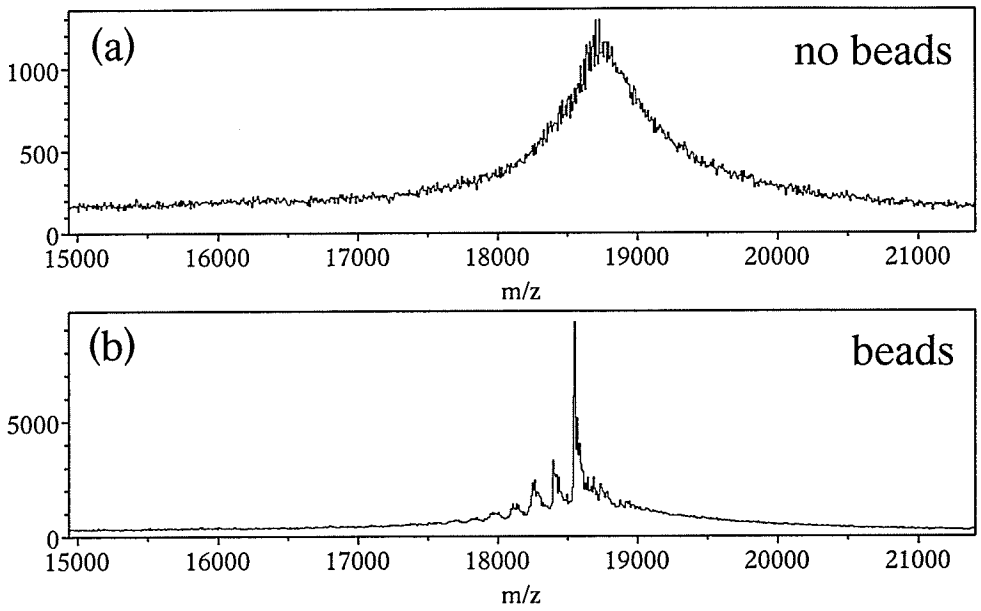


**Figure 3-12.** UV-MALDI mass spectra of 60-mer DNA obtained at 1 Torr with no ion exchange beads (a) and with ion exchange beads (b). The matrix used in this analysis was 3-HPA.

The heaviest DNA analyzed in the QqTOF instrument with UV excitation was a 90-mer, with a molecular weight of 27,743 Da, Fig. 3-13. The signal-to-noise ratio is poor, nevertheless the effective mass resolution at FWHM is about 900.

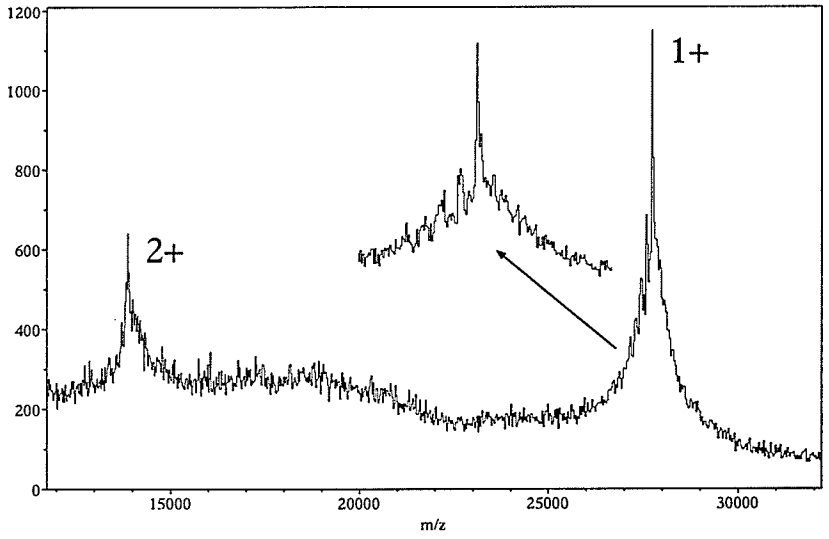


**Figure 3-13.** UV-MALDI mass spectrum of 90-mer DNA obtained at 1 Torr with ion exchange beads, the matrix used in this experiment was 3-HPA.

## 3.4 Discussion

The infrared laser from Bioptics produces a pulse of energy that is 60 times more energetic that the pulse energy from the nitrogen laser. The resulting fluence from the IR laser radiating the same is also 60 times larger, if the spot size remains constant. The larger fluence produces a bigger plume of ions and hence increases the pressure in the immediate vicinity of the target. The larger density of analyte and matrix molecules produces cooler and more stable ions, since the probability of an analyte colliding and loosing some of its kinetic energy to matrix molecule or buffer gas is increased. In IR excitation the fragmentation is minimal and independent of the buffer gas pressure near the ion source.

The interaction and bonding of the matrix molecules with the analyte is also larger due to greater plume density. The degree of matrix adducts shows no difference in mass spectra when obtained at pressures of 10 mTorr or 1 Torr of buffer gas. This is because the surrounding gas has no influence on the dense expanding plume. The matrix adducts are effectively removed by declustering voltage and by increasing the temperature of the buffer gas. The reasoning is the same as in the UV-MALDI case, and the reader is directed to see Discussion 2.4.

For low mass peptides or small DNA both UV and IR lasers provide similar quality spectra but UV gives greater sensitivity. We speculate that IR excitation produced a smaller ratio of charge to neutral ions and thus IR-MALDI is not as sensitive as UV-MALDI. For this reason UV-MALDI proved to be more effective method of analyzing high mass DNA, up to ~28 kDa. Nevertheless, with either excitation it is important to tightly control laser fluence, as both base fragments and $Na^+/K^+$ adducts are produced from over-irradiance.

As the molecular weight increases (36-mer) the soft nature of IR-MALDI provides less fragmentation and hence minimizes the need for higher pressure (1 Torr or more is required for UV) in the source region. In addition the glycerol matrix provides a

more stable ion source with no sweet spots and good signal for approximately 2500 shots. In addition, IR-MALDI using a glycerol matrix, at some conditions, produces higher charge states than are observed in UV-MALDI QqTOF instrument. With the higher charge state acceptable detection efficiency is obtained without introducing a high accelerating voltage or post-acceleration.

On a practical level, UV is still a better choice due to simpler optics, greater availability of high repetition rate low-cost lasers and simpler matrix handling.

## 3.5 Conclusion

An IR-MALDI source has been tested on an orthogonal-injection TOF mass spectrometer. The most feasible matrix for IR-MALDI is glycerol mixed with ion exchange beads and when cooled down to –25°C. The glycerol matrix produced the best signal-to-noise ratio, shot-to-shot reproducibility and long lasting signal.

The degree of adduct formation produced in IR excitation is independent of the buffer gas pressure at the ion source. We have shown that it is possible to sequence short double-stranded DNA on the QqTOF instrument with both IR and UV-MALDI.

# CHAPTER 4

## High repetition rate UV lasers for MALDI

### 4.1 Introduction

The most common laser used in MALDI is a nitrogen laser such as the Laser Science ND337 with about 250 μJ of energy per pulse, and with a controlled repetition rate up to 20 Hz. Under typical conditions, the $N_2$ laser produces $>10^5$ ions per laser shot so that in an axial geometry, it is normally necessary to use a transient recorder (TR); with microchannel plate detectors, it is also necessary to suppress low mass ions to avoid detector saturation. In the orthogonal geometry, the ion plume is spread out over typically 5000 injection pulses so it is possible to use single-ion counting with a time-to-digital converter (TDC). This makes high time resolution and high repetition rate technically simpler, and completely avoids problems with detector saturation and shadowing.

In both geometries described above, there is considerable potential benefit in using a higher repetition rate laser. In particular, the data rate in MS/MS experiments with the quadrupole/TOF instrument is at present limited by the rate of ion production; an increase by one to two orders of magnitude is possible before the data system becomes saturated. In some applications of axial MALDI, particularly post-source decay (PSD), thousands of laser shots are required to produce useful spectra, so an increase in repetition rate in these cases is also clearly desirable. In addition, a higher repetition rate may allow the same acquisition time to be realized but with smaller laser spot-sizes, and therefore fewer ions produced per pulse. This may reduce problems with detector saturation and allow the use of pulse counting methods with a TDC to reduce noise level and improve resolution. In both geometries the ability to use a smaller spot (without increasing acquisition time) may be useful for imaging applications.

Unfortunately, significantly higher repetition rate nitrogen lasers are not available, and most high repetition rate Nd-YAG lasers are significantly more expensive, and in general have much less power than necessary. Assuming the fluence is the same, and that the yield scales with the area of the spot, the total ion count rate depends only on the average power of the laser.

Here we report a preliminary evaluation of three new Nd-YAG lasers that have much higher repetition rates; although the energy per pulse is considerably lower, the average power is comparable or higher. One is a low-cost frequency-tripled, passively Q-switched, Nd-YAG laser with a nominal repetition rate of 10 kHz and energy per pulse of approximately 0.25 μJ. The other two belong to a more conventional type of Nd-YAG lasers with adjustable repetition rates of one and two kilohertz with an energy of about 20 μJ and 50 μJ per pulse, respectively. In order to obtain an acceptable fluence with these lasers, it is essential to focus the beam down to a much smaller spot than is normally used with $N_2$ lasers. Thus we can test the feasibility of the configuration described above. The lasers are tested in both the axial and orthogonal geometries, using both analog and pulse-counting methods.

## 4.2 Experimental

a) NanoUV Laser:

MALDI ions were produced by a diode-pumped, passively-Q-switched Nd:YAG solid state laser (NanoUV-355 from JDS Uniphase, model NV-00111-100). The laser produces about 0.25 μJ of energy per pulse at a wavelength of 355 nm. The pulse width is less than 700 ps, and the laser operates at a frequency of about 10 kHz, corresponding to an average output power of 2.5 mW, about 5/6 that of the nitrogen laser. The output beam diameter from the laser is 0.5 by 0.5 mm with a near Gaussian beam profile and beam

divergence of less than 1 by 3 mrad full angle. The laser head is about 20 cm long with a square cross section, 4 cm on a side.

To obtain acceptable fluence for MALDI, a 10 mm focal-length lens was used to focus the laser beam, and two 100 mm focal-length plano-convex lenses arranged in infinite conjugation were used to image the focused light onto the target. The resulting spot size from these optics is calculated to be 25 μm by 40 μm limited mainly by diffraction effects. Since the target is oriented at 30° to the beam, the area of the resulting spot on the target should be approximately equivalent to 45 μm diameter circular spot, which corresponds to an expected fluence per pulse in the range of several tens of joules per square meter, which is in the range of the usual threshold for analog measurements in MALDI. The fiber-optics setup is shown in Fig. 4-1.

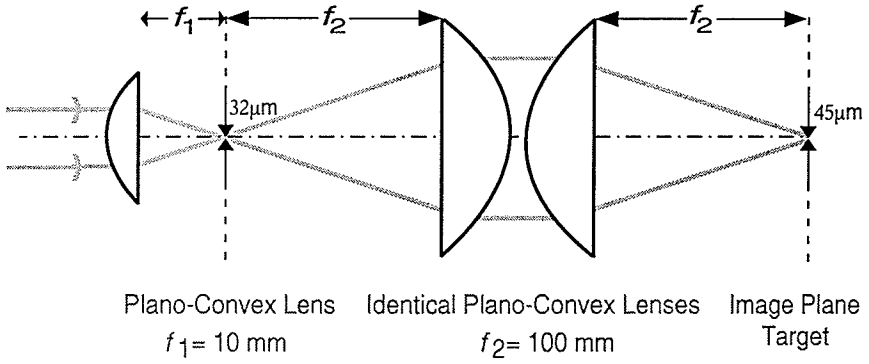


**Figure 4-1.** A schematic diagram of the optic setup used for the NanoUV laser. The beam is focused onto a target by a three-lens setup. The resulting spot size on the target is about 45 μm in diameter.

The theoretical spot size on the target created by this three-lens system can be calculated from the known divergence of the laser, and the effects of spherical aberrations and diffraction, assuming the effects are independent and add in quadrature. Initially, the spot size created by the first lens is obtained from:

$$d' = \sqrt{(f \times \phi)^2 + \left(\frac{0.067 f}{f\#^3}\right)^2 + (2.44\lambda \times f\#)^2} \qquad (4\text{-}1)$$

where $f$ is the focal length of the plano-convex lens ($f_1$ in Fig. 4-1), $\phi$ is beam divergence, and $f\#$ is equal to $f$ divided by the output beam diameter.

The light source is then imaged onto the target by a Ramsden telescope; two identical plano-convex lenses, and once again spherical aberration and diffraction must be taken into consideration. The result is show in Equation 4-2.

$$d = \frac{\sqrt{d'^2 + \left(\frac{0.067 f}{f\#^3}\right)^2 + (2.44\lambda \times f\#)^2}}{\cos\theta} \qquad (4\text{-}2)$$

where d' is the diameter of the source as calculated by using Equation 4-1, $f$ is the focal length of one of the plano-convex lens, $f\#$ is equal to $f$ divided by the effective diameter of the beam which in this case is 5 mm, and θ is the angle that the laser beam strikes the target to the normal.

b) PowerChip Laser:

The PowerChip NanoLaser (JDS Uniphase, model PNV-001025-000) is a diode pumped, all solid-state laser that produces in excess of 20 mW of average power at 1 kHz, which is about 4 times the average power of the nitrogen laser. This corresponds to approximately 20 μJ of energy per pulse at a wavelength of 355 nm. The unit uses a passive Q-switch with a high power diode bar that emits short pulses with a repetition rate of more than 1 kHz. The output beam diameter from the laser is 1.0 mm with a near Gaussian profile and beam divergence of less than 1 mrad full angle. The laser pulse width is less than 500 ps.

The energy per pulse from the PowerChip laser allows the use of fiber optics to transport the beam to the target, using the arrangement shown in Fig. 4-2. A 3-lens system was used to expand the beam before coupling into the fiber to allow the use of a neutral density filter without damaging it. The output from the fiber was then focused onto the target by a set of 120 mm lenses. The beam was oriented 65° to the normal of

the MALDI target. The resulting spot size on the target was calculated using Equation 2-1 to be roughly equivalent to a 190 μm diameter circular spot.

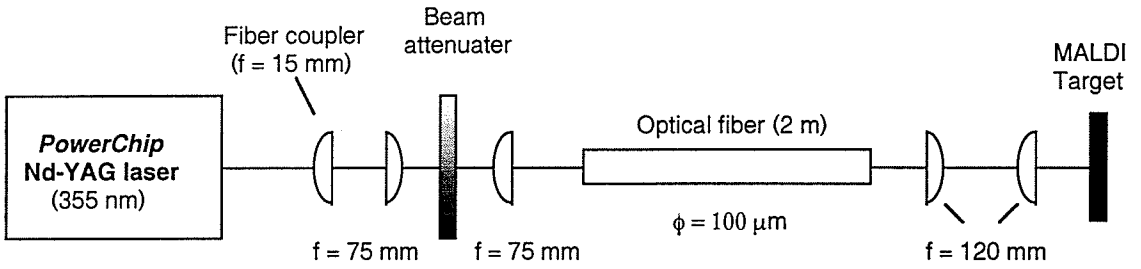


**Figure 4-2.** Fiber-optic setup used to radiate a MALDI target with a beam from a PowerChip laser. The beam is directed to an optical fiber using a 15 mm focal-length lens and two lenses arranged in infinite conjugation. The beam from the fiber is directed onto the target by two 120 mm lenses.

c) StableLight Laser:

The StableLight diode pumped Nd:YAG solid-state laser (JDS Uniphase, model S3558-100Q) operating in Q-switch mode outputs in the range of 50 - 60 μJ of energy up to 2 kHz at a wavelength of 355 nm, giving an average power of about 10 mW. The energy per pulse starts to decrease at higher operating frequency and at 5 kHz the output energy is approximately 30 μJ. The pulse width ranges from 8 to 10 ns. The beam size is 1 mm in diameter with a divergence of 2.5 mrad (full angle) and beam profile of near Gaussian.

The laser light was transported to the MALDI target by using a fiber optic setup as illustrated in Fig. 4-3. A neutral density filter was placed between the negative and a positive lens in order to attenuate the beam. The output of the fiber was imaged onto the target with two 120 mm lenses. Again, the beam was oriented at 65° to the normal of the MALDI target. The resulting spot sizes on the target were equivalent to circular spots with diameters of about 190 μm and 330 μm (again Equation 2-1 was used) for the 100 μm and 200 μm fiber, respectively.

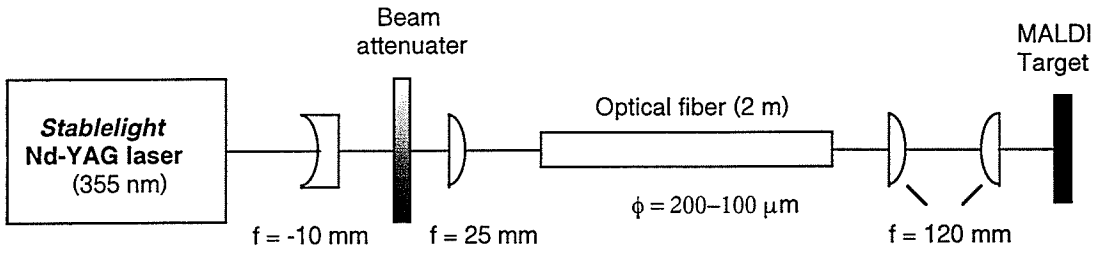


**Figure 4-3.** A schematic diagram of a fiber-optic setup used to image the beam from a StableLight laser onto a target. The beam is directed to an optical fiber using a -15 mm and 75 mm focal-length lenses. The beam from the fiber is then imaged onto the target by two 120 mm lenses.

d) Nitrogen Laser:

An $N_2$ laser (VSL-337ND from Laser Science Inc.,) with a controlled repetition rate of up to 20 Hz, normally used in our laboratory for UV-MALDI, and the most common laser used for MALDI, was used for comparison. When the $N_2$ laser is used under normal conditions it produces a spot size equivalent of about 300 μm in diameter with fluence on the order of 100 J/m$^2$. To make the comparison more direct, the laser beam was also focused with the three-lens setup used for NanoUV laser (see Fig. 4-1) to give a spot size on the target equivalent to circular spots with diameters of about 150 μm with fluence adjusted to give useful spectra. The $N_2$ laser produces approximately 250 μJ per pulse for 3 ns at a wavelength of 337.1 nm with an output beam size of 40 square mm and beam divergence of less than 0.3 mrad.

e) Mass spectrometry

All mass spectra were acquired with two instruments; a simple axial-injection TOF-MS without an ion mirror, and an orthogonal injection quadrupole TOF-MS with an ion mirror (QqTOF). The axial TOF has a flight length of about 80 cm and an extraction region of approximately 4 cm with an acceleration voltage of 15 kV. A microchannel plate detector and an integrating transient recorder (ITR-model 9846B) with 9826AV

summation average from Precision Instruments, Inc. (Knoxville, Tennessee) was used to collect the data. Some measurements were also made with a time-to-digital converter (TDC). In addition, deflection plates located about 35 cm from the target were used to suppress the low mass ions. A schematic diagram of the axial TOF is shown in Fig. 4-4.

The orthogonal injection quadrupole TOF mass spectrometer (QqTOF) has been described in detail in Chapter 2. However, in this experiment it is important to point out that QqTOF instrument uses a 4-anode microchannel plate detector and a 4-channel TDC for the acquisition system.

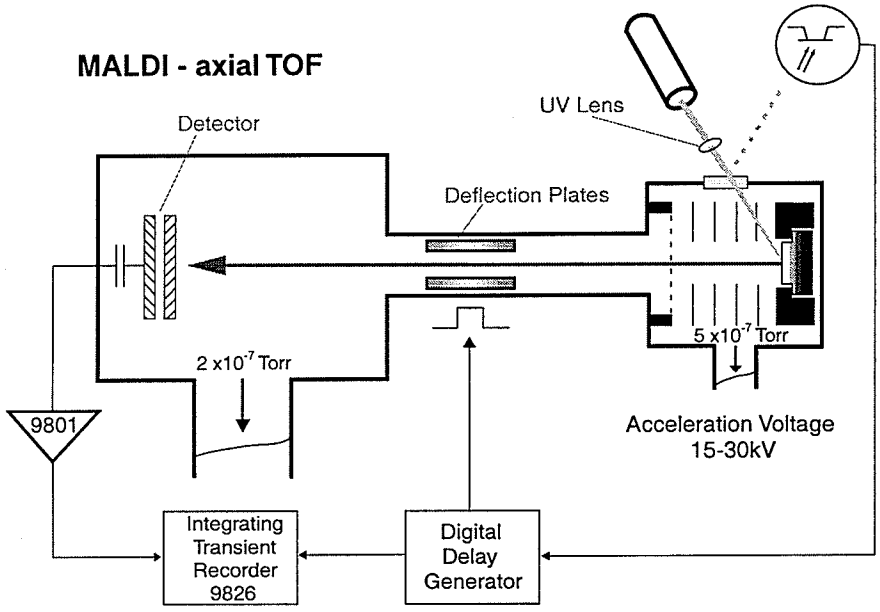


**Figure 4-4.** A schematic diagram of a MALDI-axial time-of-flight mass spectrometer.

f) Sample preparation:

Samples were prepared by depositing 1 μL of a saturated matrix solution on a stainless steel probe. Once the layer of a matrix was dried, 1 μL of pre-formed mixture of 9 μL of a matrix solution plus 1 mL of analyte solution (4 g/L) was applied on top of the crystallized matrix. Analyte solutions were dissolved with a 0.1% aqueous trifluoroacetic

acid (TFA). The matrices, 2,5-dihydroxy-benzoic acid (DHB) and alpha-cyano-4-hydroxicinnic acid, were prepared using a 0.1% TFA and acetonitrile (2:1v/v) mixture. All analyte and matrices were purchased from SIGMA.

## 4.3 Results

a) Axial -TOF

For a first investigation, we wanted to determine the feasibility of using a compact, inexpensive NanoUV laser for the usual axial MALDI experiment. Since the repetition rate is very high, the usual transient recorder is not suitable, so experiments were done either in the analog mode with an integrating transient recorder (ITR) or with a time-to-digital converter (TDC) in pulse-counting mode.

Good quality mass spectra were obtained with an integrating transient recorder, but this required considerable trial and error, because at 10 kHz the sample was quickly exhausted. Fig. 4-5 shows a spectrum acquired in one second although in principle much less time is required since a only small fraction of the many recorded shots contribute useful data.

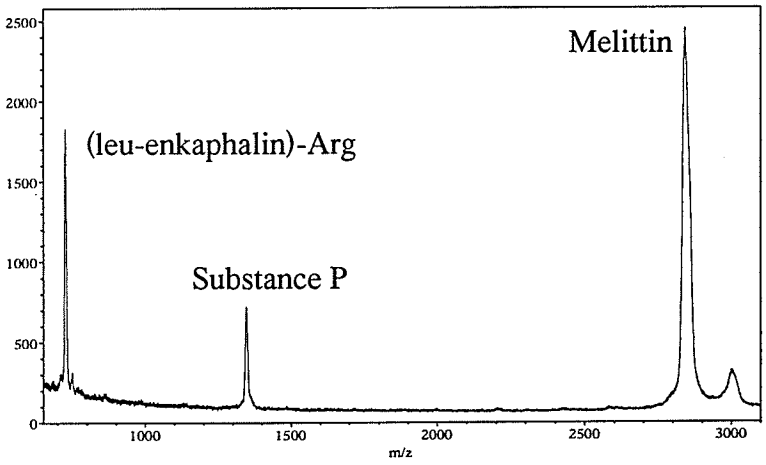


**Figure 4-5.** Mass spectrum of a mixture of peptides obtained on an axial instrument from an DHB matrix. The repetition rate of the NanoUV laser was 10kHz.

The unusual spectrum of cytochrome C shown in Fig. 4-6 illustrates the problem of including many shots that contain only noise; the spectrum is shown with a large constant background subtracted. Lysozyme, with *m/z* of about 14,306 Da, was the heaviest protein observed with this technique, see Fig. 4-7. Thus, while it is possible to get spectra from small proteins with this laser, using similar sample preparation methods, the spectral quality is significantly poorer, and more difficult to obtain.

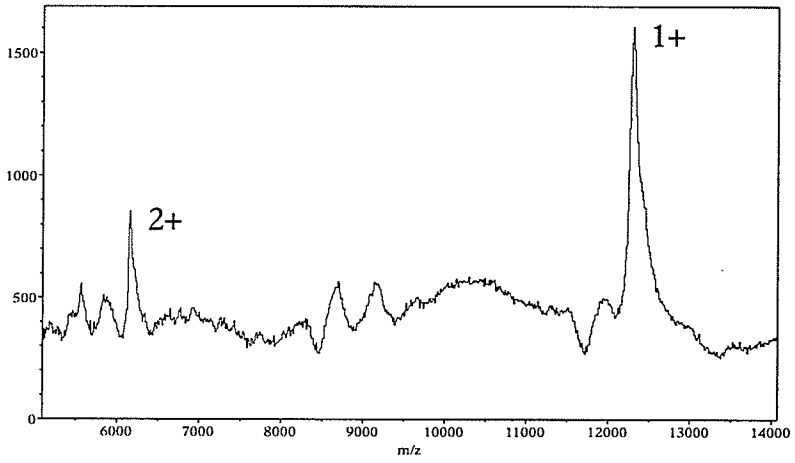


**Figure 4-6.** MALDI spectrum of singly and doubly charged cytochrome C obtained using the NanoUV laser on the axial instrument. The spectrum was acquired with the DHB matrix.

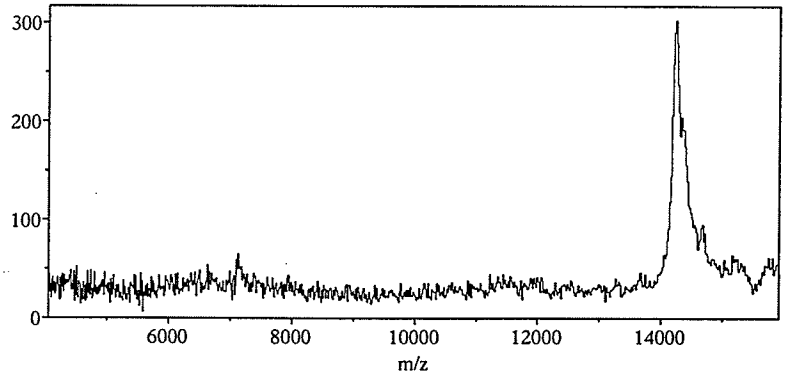


**Figure 4-7.** Mass spectrum of singly charged lysozyme obtained using the NanoUV laser on the axial instrument, with large constant background subtracted. The intensity of the doubly charged lysozyme is very low, and almost fades in the background noise. DHB matrix was utilized and the laser repetition rate was 10kHz.

Besides the difference in repetition rate and energy per pulse with this laser, the spot size is also significantly smaller as described in detail in the experimental section, so the possibility that this difference plays a role was also considered. To determine the effect of spot size on the spectrum, the same three-lens setup as described in the experimental section for the NanoUV laser, was also used with the nitrogen laser. With this optics, the area of the spot from the nitrogen laser was reduced by at least a factor of 4, limited by aberration due to the relatively large beam diameter. The spectrum obtained for cytochrome C is shown in Fig. 4-8. It was acquired in 13 seconds with relative ease and good reproducibility. The quality of the spectrum including resolution and relative intensity is comparable with if not better than the spectra obtained with the usual optics, so spot size does not appear to be a significant factor.

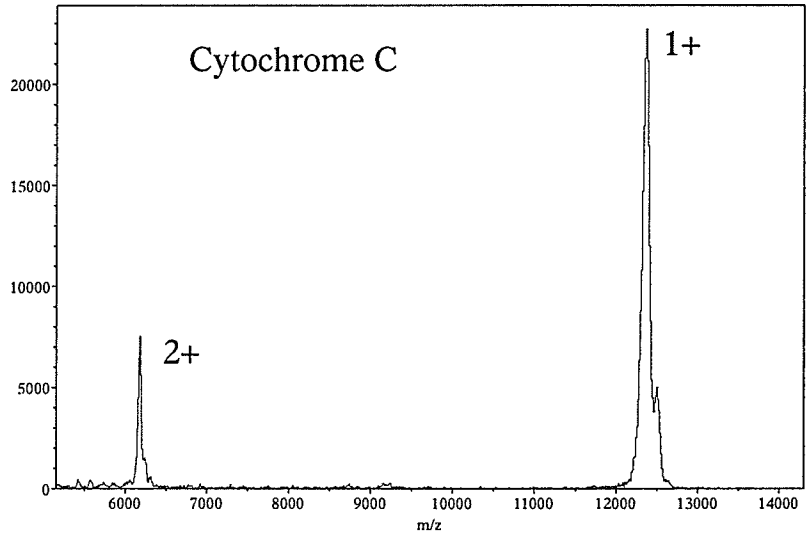


**Figure 4-8.** Spectrum obtained from cytochrome C in the axial spectrometer with $N_2$ laser and the three-lens setup that produces a spot size on the MALDI target of about 150 μm in diameter. DHB was used as the matrix.

In the pulse-counting experiments with a single channel TDC useful spectra of peptides and proteins were not obtained. Although the average number of ions per pulse is quite small, it is likely that most of the ions were produced in a small fraction of the laser pulses [1]. Therefore, a single-anode detector does not appear to be suitable for

pulse-counting methods with this laser, but the possibility of using a multi-anode (64 or more) detector with a multi-channel TDC has not been excluded.

b) Orthogonal-TOF

The results obtained in the QqTOF instrument were much more promising. The injection pulse rate in this instrument is similar to the laser repetition rate, so ideally the average number of ions would be similar to the data obtained with axial TOF. But the QqTOF introduces considerable attenuation and perhaps more importantly smoothes out the variation in the number of ions per pulse and allows a 4-channel TDC to be used. Fig. 4-9 shows the spectrum of a mixture of peptides, which was acquired with the NanoUV laser in approximately 30 seconds with comparable ease and reproducibility to that of the 20 Hz nitrogen laser and with comparable count rate and sensitivity. Fig. 4-10 shows a spectrum of cytochrome C without background subtracted; the highest protein observed was trypsinogen (~ 24 kDa). In this mass range the nitrogen laser performs somewhat better, but for both lasers the low acceleration voltage (10 kV) limits the performance.

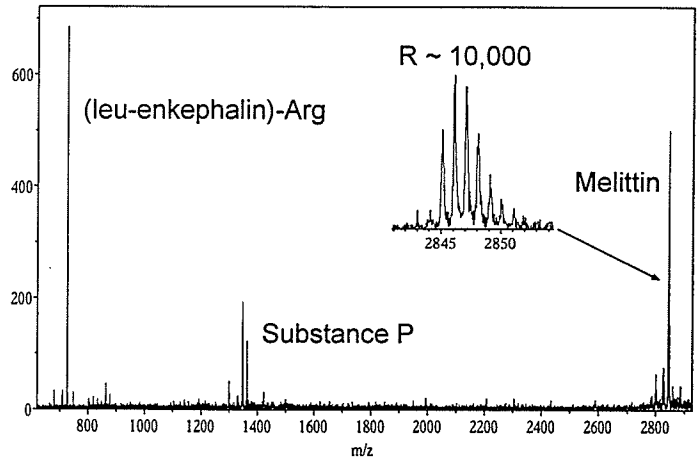


**Figure 4-9**. Mass spectrum of (leu-enkephalin)-Arg, substance P and melittin. The spectrum was obtained with the QqTOF instrument using the NanoUV laser. DHB was used as the matrix.

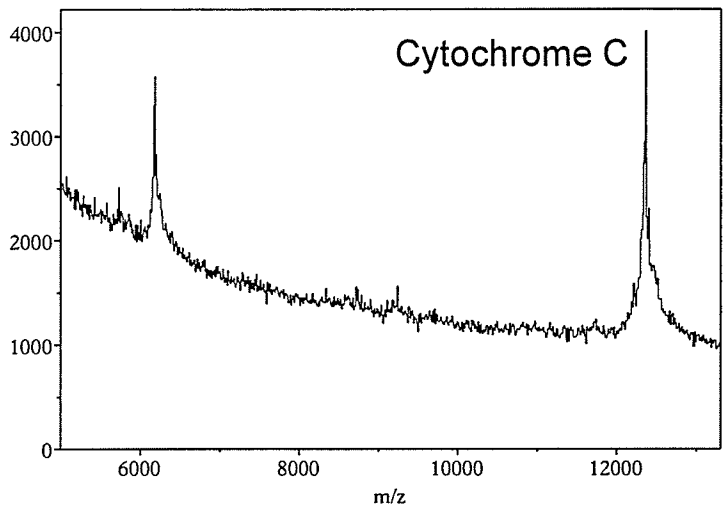


**Figure 4-10**. Mass spectrum of cytochrome C obtained with the QqTOF instrument using the NanoUV laser and DHB matrix. The resolution at full width half maximum of the parent ion is 1100.

The NanoUV laser in its present form is already competitive with the usual nitrogen laser in the orthogonal geometry. However, a modest increase in power would provide significantly higher count rates than are possible with nitrogen lasers, and for significantly less expense than conventional high repetition rate Nd:YAG lasers. Acquisition times for MS/MS measurements in the QqTOF instrument while significantly shorter than PSD measurements in the axial geometry are still limited by the rate of ion production.

For this reason we have tested the StableLight laser. The energy per pulse is about 5 times lower than the $N_2$ laser but 200 times more powerful than the NanoUV laser. Since the energy of the StableLight laser is lower than the $N_2$ laser three-lens optics was required, as described in the experimental section, in order to focus the beam for acceptable fluence. The repetition rate can be increased to several kHz, but the laser can also be run in a low repetition rate mode for measuring single-MS spectra.

We have measured the MS and MS/MS spectra from a 50 fmol sample of fibrinopeptide A using the StableLight laser. The single-MS spectrum of the 1536 Da peptide was obtained in 5 seconds, running this laser at 15 Hz. An MS/MS spectrum from

the same spot, taken in 7 seconds at a laser repetition rate of 500 Hz, is shown in Fig. 4-11. The mass accuracy for MS/MS measurements in this high throughput mode appears to be comparable to the accuracy at low throughput (20 Hz with $N_2$ laser), within 10 mDa (or 10 ppm) in nearly every case. Very little chemical or detector noise is observed in this MS/MS spectrum, so only a few ions are necessary to identify a peak. This can be seen in the inset in Fig. 4-11 where even small peaks like $b_4$ (34 counts) and $y_3$ (47 counts) are well represented and clearly resolved at the same nominal mass (mass difference between the two peaks $\Delta M = 0.090$ Da, $\Delta M/M = 270$ ppm).

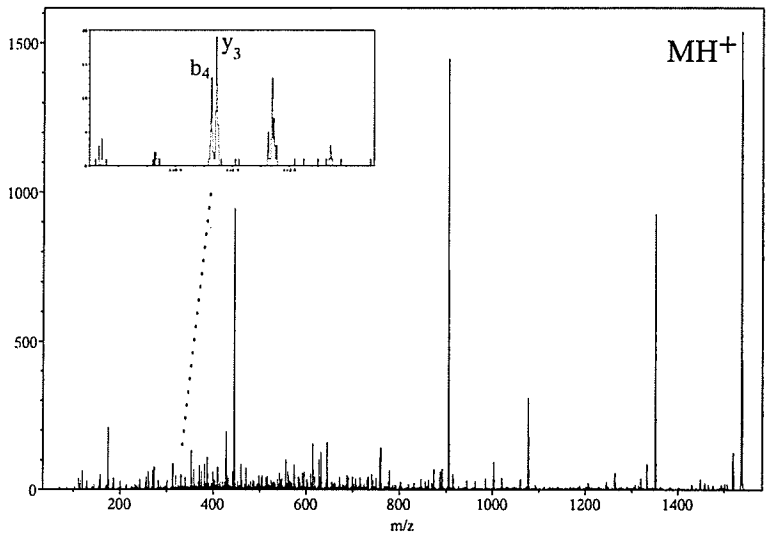


**Figure 4-11.** MS/MS spectrum of fibrinopeptide A, acquired from 50 fmol of sample in 7 seconds using a laser repetition rate of 500 Hz. The data is displayed in 0.625 ns bin.

Although the StableLight appears to be well suited to the QqTOF experiment, it is no longer available commercially, so we also tested a somewhat lower power (but also less expensive) PowerChip laser (see Experimental). This laser with repetition rate up to 1 kHz was evaluated for MALDI. PowerChip yields approximately 80 times the energy per pulse as compared to the NanoUV laser. The PowerChip produces good quality MS and MS/MS data. A typical mass spectrum of cytochrome C obtained with the power chip laser from DHB matrix is shown in Fig. 4-12. The spectrum was acquired in just over a minute with good reproducibility and good signal to noise ratio. Myoglobin, was

the heaviest protein analyzed with the power chip laser, see Fig 4-13. Even at high mass (~16 kDa) the PowerChip laser performs just as well as the nitrogen laser.

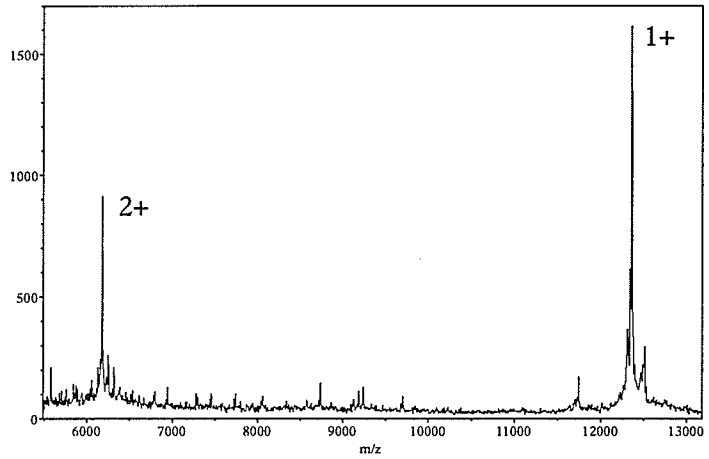


**Figure 4-12.** A single mass spectrum of cytochrome C from DHB matrix. The data was acquired in one minute at a repetition rate of 10 Hz using a power chip laser.

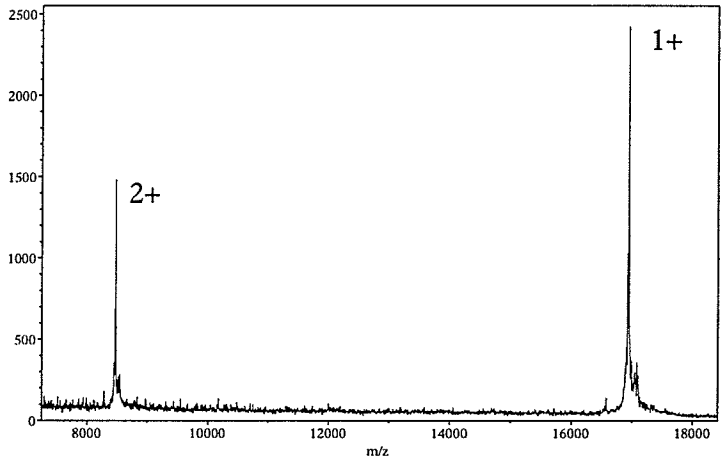


**Figure 4-13.** Mass spectrum of myoglobin from DHB matrix. The data was acquired in just over one minute at a repetition rate of 50 Hz using a power chip laser. 40 pmol of the analyte was deposited on the target.

The expectation in using higher repetition rate lasers is that the count rate simply scales with repetition rate, assuming the laser energy is independent of repetition rate, and can be rastered in such a way that the sample use is comparable, and that each desorption event is independent. These assumptions were tested using the PowerChip laser by measuring number of ions in a selected mass range versus repetition rate. To perform these experiments insulin with alpha-cyano-4-hydroxicinnic acid and/or DHB

matrix was used. The experimental data indicated by the solid lines in Fig. 4-14 was obtained by gradually increasing the frequency of the laser. The predicted data shown by the dashed lines was obtained by scaling the initial intensity by frequency. The intensity at a given frequency was obtained by integrating both singly and doubly charged insulin ions. In either case the integral over the 1+ and 2+ mass range show to be linear with the repetition rate. The results indicate that the assumptions are reasonably valid, at least up to about 100 Hz, but seem to break down at higher frequencies. This is most likely due to the known decrease in energy per pulse at higher repetition rates.

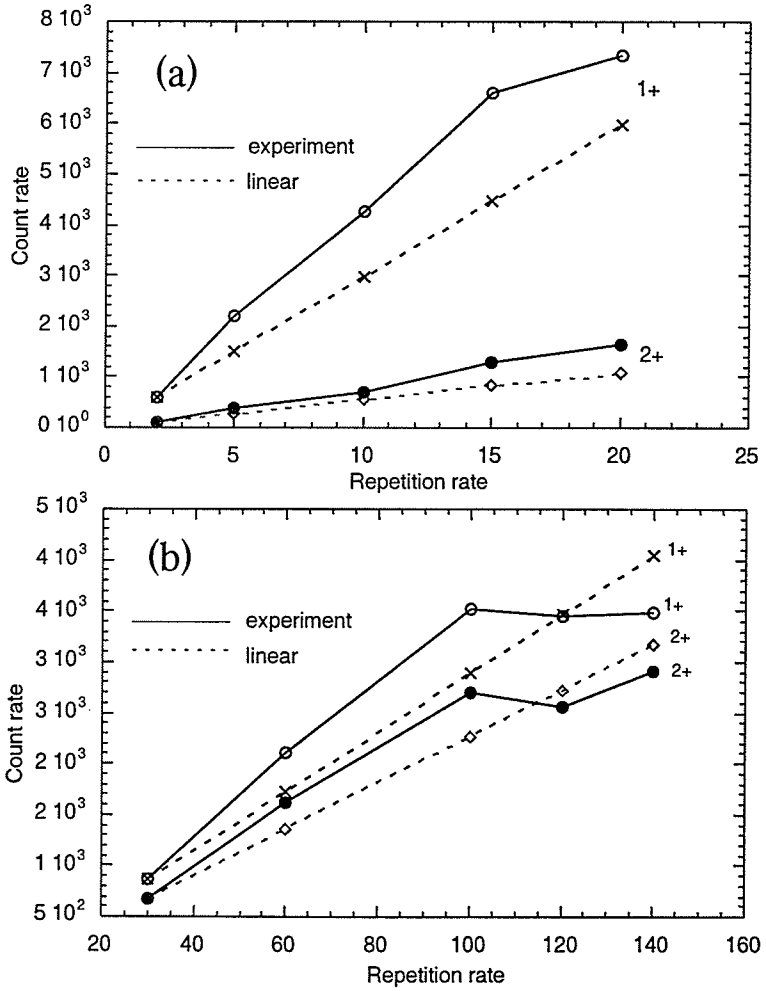


**Figure 4-14**. A graph of the counts per *m/z* range versus frequency obtained from insulin using (a) alpha-cyano-4-hydroxicinnic acid matrix and (b) DHB matrix. The solid line indicates the experimental data and the dash line denotes the predicted number of counts. 1+ and 2+ are the singly and doubly charged states of the insulin ion.

## 4.4 Discussion

A new diode-pumped, passively-Q-switched Nd:YAG (NanoUV) laser, with a wavelength of 355 nm, has been evaluated for use in MALDI in an axial and orthogonal-injection time-of-flight mass spectrometer. In the linear TOF instrument the NanoUV laser gives poor spectra with the TDC especially for higher *m/z* range, which is due to very low signal to noise ratio. Better results were obtained with ITR. In the orthogonal geometry the NanoUV laser performs similarly as the $N_2$ laser. The count rate, sensitivity, reproducibility and ease of obtaining good spectra are comparable for both lasers. However, for MS/MS measurements in the QqTOF instrument a NanoUV laser with increased power and thus a higher count rate is particularly desirable. The target must be scanned to avoid quick exhaustion of the sample for both instruments. In its present form, this laser has limited applications, except possibly in imaging. If in the future the laser power were increased and the repetition rate could be controlled, the NanoUV laser may be useful for MALDI.

The NanoUV laser also has potential advantages for imaging applications because a microscopic beam spot can be produced, while maintaining the same count rate. Even in an axial TOF instrument, the faster spectrum acquisition may be exploited if higher power and better control of the repetition rate is achieved.

A StableLight laser with 200 times more energy per pulse than the NanoUV laser was utilized for MS/MS analysis. With this high-repetition rate laser, both single-MS and MS/MS spectra can be acquired in a few seconds from the same sample spot. This allows an intelligent, iterative process to be used for protein identification with maximum economy for both sample and time [2]. However, the StableLight laser is no longer commercially available due to high cost and poor reliability. As a result the StableLight laser has been replaced with a much more dependable and lower cost PowerChip laser.

PowerChip laser proved to be the most practical high repetition rate laser for analysis of biomolecules in MS and MS/MS mode. The PowerChip laser provides the

ability to sequence proteins in just a few seconds. The laser has sufficient energy per pulse and the ease of use to replace the typical nitrogen laser used for MALDI.

# REFERENCES

## Chapter 1


[1] Karas, M.; Hillenkamp, F. *Anal. Chem.* **(1988)**; *60*, 1299.

[2] Tanaka K., Waki H., Ido Y., Akita S. and Yoshida Y. *Rapid Commun. Mass Spectrom.* 2 **(1988)** 151.

[3] Hillenkamp F., Karas M., Beavis R.C. and Chait B.T., *Anal. Chem.* **63 (1991)** 1193A.

[4] Vertes A., In *Methods and Mechanisms for Producing Ions from Large Molecules;* Standing K.G. and Ens W., Eds.; NATO ASI Series B: Physics Vol 269.; Plenum Press, New York, **(1991)**, pp 275-291.

[5] Wang B.H., Dreisewerd K., Bahr U., Karas M. and Hillenkamp F. *J. Am. Soc. Mass Spectrom.* **(1993)**, *4*, 393-398.

[6] Johnson R.E., *Int. J. Mass Spectrom.* **(1994)**, *139*, 25-38.

[7] Ens W., Mao Y., Mayer F. and Standing K.G. *Rapid Commun. Mass Spectrom.* 5 **(1991)** 117-123.

[8] Fenn J.B., Mann M., Meng C.K., Wong S.F. and Whitehouse C.M. *Science* **(1989)**; *246*, 64.

[9] Aleksandrov, M.L.; Gall, L.N.; Krasnov, N.V.; Nikolayev, V.I.; Pavlenko, V.A.; Shkurov, V.A. *Dokl. Phys. Chem.* **1985,** *277,* 572-76.

[10] Torgerson D.F., Skowronski R.P. and Macfarlane R.D. *Biochem. Biophys. Res. Commun.* **1974**, *60,* 616-21.

[11] Mamyrin B. A., Karatajev V. J., Shmikk D. V., and Zagulin V.A. *Sov. Phys. JETP* **1973**, *37*, 45-48.

[12] Tang X., Beavis R., Ens W., Lafortune F., Schueler B. and Standing K.G., *Int. J. Mass Spectrom. Ion Processes* **1988**, *85*, 43.

[13] Wiley W.C. and McLaren I.H. *Rev. Sci. Instrum.* **1955,** *26,* 1150.

[14] Vestal M., reported at the *Sanibel Conference on Mass Spectrometry*, Sanibel Island, FL, 24-27 January, 1998.

[15] Dodonov, A.F.; Chernushevich, I.V.; Laiko, V.V. In *Time-of-Flight Mass*

*Spectrometery;* Cotter, R. J., Ed.; American Chemical Society Symposium Series 549; Washington, DC, **1994,** 108-23.

[16] Verentchikov A.N., Ens W. and Standing K.G. *Anal Chem* **1994**, 66, 126.

[17] Krutchinsky, A.N.; Loboda, A. V.; Spicer V.L.; Dworschak, R.; Ens, W.; Standing, K.G. *Rapid Commun. Mass Spectrom.* **1998;** *12*; 508-18.

# Chapter 2

[1] A. Verentchikov, I. Smirnov, M. L. Vestal, Proc 47th ASMS Conf. *Mass Spectrom. and Allied Topics*, Dallas, Texas (1999); 3052-3053.

[2] Chernushevich IV, Ens W, Standing KG, *Anal. Chem.* 1999; **71:** 452A.

[3] Shevchenko A, Chernushevich IV, W Ens W, K G Standing KG, B Thomson B, M Wilm M, and M Mann M, *Rapid Commun. Mass Spectrom.* 1997;**11**: 1015.

[4] Krutchinsky AN, Loboda AV, Spicer VL, Dworschak R, Ens W, Standing KG, *Rapid Commun. Mass Spectrom.* 1998;**12**: 508.

[5] Loboda AV, Koslovski VI, Chardakova EV, Tolmachev AV, Sulimenkov IV, Dodonov AF, Wollnik H, *Rapid Commun. Mass Spectrom.* 1998;**12**: 45;

[6] Covey T, Douglas DJ, *J Am. Soc. Mass Spectrom.* 1993; **4**: 616.

[7] K. Dreisewerd, M. Schurenberg, M. Karas, F. Hillenkamp *Inter. Mass Spectrometry and Ion Processes* 141, (1995) 127-148.

[8] M. Thierolf, U. Bahr, M. Karas, Proc 45th ASMS Conf. *Mass Spectrom. and Allied Topics*, Palm Springs, California (1997); 856 .

# Chapter 3

[1] S. Berkenkamp, F. Kipekar, and F. Hillenkamp, *Science* (1998), **281**, 260-262.

[2] A. Overberg, M. Karas, U. Bahr, R. Kaufmann and F. Hillenkamp *Rapid Commun. Mass Spectom.* (1990) **4**, 293-296.

[3] A.V. Loboda, A.N. Krutchinsky, M. Bromirski, W. Ens and K.G. Standing *Rapid Commun. Mass Spectrom.* (2000) **14**, 1-11.

# Chapter 4

[1] J. Zhou, W. Ens, K. G. Standing and A. Verentchikov *Rapid Commun. Mass Spectom.* (1992) **6**, 671-678.

[2] A. Shevchenko, A. Loboda, A. Shevchenko, W. Ens, K.G. Standing, *Anal Chem*, (2000) **72**, 2132-2141.